1 3 0

REPORT DOCUMENTATION PAGE

AFRL-SR-BL-TR-98-

0117

sources, t of this efferson

1. AGENCY USE ONLY (Leave Blank)	2. REPORT DATE 1/5/98	3. REPORT TYPE AND DATES COVERED Final 9/94 – 9/97

4. TITLE AND SUBTITLE
Site-Selective Spectroscopy of Adsorbates on Mineral Surfaces using FTIR

5. FUNDING NUMBERS
F49620-94-1-0419

PR/TA 3484/BS

6. AUTHORS
Keith T. Carron

7. PERFORMING ORGANIZATION NAME(S) AND ADDRESS(ES)
University of Wyoming
Department of Chemistry
P.O. Box 3838
Laramie, WY 82071-3838

8. PERFORMING ORGANIZATION REPORT NUMBER

5-31862

9. SPONSORING / MONITORING AGENCY NAME(S) AND ADDRESS(ES)
AFOSR
110 Duncan Avenue, Suite B115
Bolling AFB, DC 20332-8080

N/A

10. SPONSORING / MONITORING AGENCY REPORT NUMBER

11. SUPPLEMENTARY NOTES

12a. DISTRIBUTION / AVAILABILITY STATEMENT

unlimited

12b. DISTRIBUTION CODE

13. ABSTRACT (Maximum 200 words)
see next page

14. SUBJECT TERMS
Raman Spectroscopy, Infrared Spectroscopy, Modeling, Modified Clays

15. NUMBER OF PAGES
64

16. PRICE CODE

17. SECURITY CLASSIFICATION OF REPORT	18. SECURITY CLASSIFICATION OF THIS PAGE	19. SECURITY CLASSIFICATION OF ABSTRACT	20. LIMITATION OF ABSTRACT

19980129 054

SPECTROSCOPIC STUDIES OF CLAY MODIFIERS & METAL ION-HUMIC ACID INTERACTIONS

ABSTRACT

The montmorillonite clay modification was studied by DRIFTspectroscopy. The modifiers we used were the nonionic modifiers n-heptadecanonitrile (C_{16} nitrile) and hexadecanamide (C_{16} amide) which are biologically inert and degradeable. The interaction mechanisms between these modifiers and the montmorillonite clay were investigated. It is found that the polar groups of the modifiers can interact with the specific $Si^{\delta+}$-$O^{\delta-}$-M^{n+} structure of montmorillonite through dipole-ion and dipole-dipole interactions to form a stable complexes. The investigation of a possible hydrolysis of C_{16} nitrile on the montmorillonite interlayer surface indicated that at a strong acidic condition, the C_{16} nitrile can be hydrolyzed to form C_{16} amide which interacts with the montmorillonite clay interface to form a stable ring structure. These results are desirable in the possible application of the modified montmorillonite clay as a waste water treatment agent.

The structure of Aldrich humic acid (AHA) and its metal coordination ability are investigated by transmittance Fourier Transform InfraRed (FTIR) spectroscopy, isotopic substitution and reactive substitution were used to assign the IR spectra. A characteristic redox reaction and model compounds were also used for studying a macromolecular AHA. Structure studies have indicated that catechol analogues and phthalic acid analogues are the main functional groups of AHA. It was found that the metal coordination ability of AHA was affected by functional group's characteristics and solution pH. AHA showed higher metal coordination ability at neutral conditions than that at acidic conditions. Catechol analogues coordinate with metal cations to form metal - semiquinone complexes through an oxidation-chelation mechanism. In order to better understand the complex chemistry of AHA, we chose catechol as the model compound and investigated its structure and metal coordination properties at the same conditions as that for AHA. It was found that the catechol model compounds have macromolecular characters due to its polymerization, which is reminiscent of what is seen with AHA. Both catechol model compounds and AHA have mainly similar active functional groups and similar metal coordination characteristics making catechol appears to be an acceptable model compound for the study of AHA.

TABLE OF CONTENTS

LIST OF FIGURES

LIST OF TABLES

LIST OF ABBREVIATIONS

FTIR- Fourier Transform Infrared

DRIFT- Diffuse Reflectance Infrared Fourier Transform Spectroscopy

C$_{16}$ Nitrile - n-Heptadecanonitrile

C$_{16}$ Amide - Hexadecanamide

SOM- Soil Organic Matter

HA-Humic Acid

AHA- Aldrich Humic Acid

Humate -Humic Acid Salt

K$_{ow}$ -Octanol / Water Partitioning Coefficient

Condition I-Solution pH=1 and 60-70^0 C Temperature

Condition II-Solution pH=1 and Room Temperature

Condition III-Solution pH=6 or 7 and Room Temperature

CHAPTER I

Introduction

1.1 Motivation

Inorganic and organic contaminants in ground water may constitute significant health hazards. Often natural remediation processes are too slow to provide adequate removal of wastes. Two natural materials, humic acid (HA) and montmorillonite clay, are common sorbants of contaminants. HA is part of the soil organic matter (SOM) which can absorb or interact with a variety of organic and inorganic contaminants including benzene and metal ions such as Cr^{6+}, Fe^{3+}, and Cu^{2+} in the subsurface.[1] The aqueous concentration and transport of these hazardous organic and inorganic compounds in the groundwater can be profoundly affected by their sorption and complexation to HA.[2,3] Montmorillonite, one of the common clay minerals, contains a reactive interlayer. The chemical characteristics of the interlayer can be controlled by organic modifiers through characteristic interactions such as ion exchange, ion paring, dipole-dipole interaction, dipole-ion interaction, and hydrogen bonding between hydrophilic head groups of modifiers and specific sites on the interface. These modifications can improve the clay's organic contaminant sorption capability.[4,5]

This research proposal is divided into two parts. In the first part, we use Diffuse Reflectance Infrared Fourier Transform (DRIFT) spectroscopy to study montmorillonite modification by the nonionic modifiers, n-heptadecanonitrile (C_{16}-nitrile) and hexadecanamide (C_{16}-amide). The study includes examination of the modifier-montmorillonite complexation mechanism and stability of the complexes. The most important advantages of the nonionic modifiers include a significantly lower sensitivity to the presence of electrolytes in the environment, a diminished dependence on solution pH, and the synthetic flexibility.[4,5] In addition, nonionic modifiers are low toxic to bacteria in comparison with ionic modifiers.[4,5] Therefore, the use of C_{16} nitrile and C_{16} amide as clay modifiers does not create new environmental contamination in the process of removing existing waste. Early work in mineral surface modification mainly focused on cationic modifiers because cationic heads of modifiers can easily exchange with surface bound metal ions of minerals. It was found that this modification was sensitive to the presence of electrolytes in the system and affected by solution

1

pH. The synthesis of ionic modifiers required careful control of the size of hydrophilic groups to create a desired degree of solubility in the water.[4] In addition, ionic modifiers are biologically active and can kill or inhibit the growth of many microorganisms.[4] In our work, we examined nonionic modifiers to modify the mineral surface to reduce the disadvantages of ionic modifiers and to give a stable, low toxic, and biodegradable organo-clay.

In the second part of this research, we use Aldrich humic acid (AHA) as an inexpensive, commerically available representative of natural HA. The structure of AHA was investigated by Fourier Transform Infrared (FTIR) spectroscopy. Deuteration, characteristic redox reaction, and a targeted chemical reaction were used to simplify the FTIR spectrum interpretation. The metal coordination ability of AHA was determined under different pH solutions. The metal coordination mechanism of AHA was also studied. Previously, soil science has characterized the sorption of organic species onto SOM using K_{ow} (octanol / water partitioning coefficient).[6] K_{ow} is meant to simulate sorption in a predictable manner. In our study, we try to understand the metal contaminant sorption mechanisms in AHA by characterizing and simulating the functional groups found in the AHA. We believe this microscopic view of the sorption will provide a better understanding of the natural sorption process which occurs in the groundwater systems.

1.2 DRIFT and FTIR Spectroscopy Theory

FTIR is employed for structural analysis of compounds. Most natural and synthetic compounds we used are insoluble polymers. This made transmittance FTIR and DRIFT the methods of choice. DRIFT is specially used for powder samples and is suited for the study of organo-clay powders.

Vibrational spectroscopy is suited for the study of organo-clays and HA material. It is a fingerprint technique and, therefore, is able to provide information about large, complicated molecules. Infrared absorptions arise from changes in a bond or group dipole moment due to vibrations of that bond or group. The vibrational frequency is given by Hooke's law: [7]

$$v = \frac{1}{2\pi}\sqrt{\frac{F}{\mu}} \qquad\qquad (1)$$

where μ is given by

2

$$\frac{1}{\mu} = \frac{1}{m_1} + \frac{1}{m_2} \qquad (2)$$

m_1 and m_2 are the mass of the two atoms, respectively, and F is the force constant for the bond.

We made use of Hooke's law to help elucidate the structure of our organo-clays, AHA complexes, and HA mimetics through isotopic substitution. Since ν in Equation (1) is dependent on the reduced mass, μ, and μ is dependent on the atomic masses of the atoms involved in the vibration, it is possible to shift specific vibrations through isotopic substitution. This feature of vibrational spectroscopy allowed us to determine which vibrational features were due to exchangeable protons. Similarly, it also allowed us identify the functional groups by studying the band shift from that of original species to that of derivatives. For example, this made it possible to determine if a catechol had been oxidized to a quinone. In AHA this is very important due to the natural abundance of carbonyl groups from carboxylic acids.

1.3. ESR Spectroscopy

ESR spectroscopy can be used to detect radical species. In our work, we specifically detected the semiquinone radical and metal ion in metal ion-AHA complexes by ESR spectroscopy for investigation of the interaction mechanism between metal ions and functional groups of AHA.

The basic phenomenon underlying ESR spectroscopy is the Zeeman effect. This involves an interaction between the spin of an unpaired electron and an external magnetic field. In the absence of a field, the energy of the electron degenerate or in other words it is independent of whether its spin is +1/2 or -1/2. In the presence of a field of strength H_o, however, the Zeeman interaction leads to the following relationship: [8]

$$E = -g\beta M_z H_o \qquad (3)$$

where E is the energy of the unpaired electron, g is the spectroscopic splitting factor, which is 2.00229 for "free spin" (not influenced by any magnetic nuclei), β is the Bohr magneton (a constant) and M_z is the

component of spin angular momentum of the electron in the direction of the applied field, H_o (z axis).

Because M_z may have values of +1/2 or -1/2, the alignment of the spin magnetic moment may be either with the magnetic field direction (low energy) or against the magnetic field direction (high energy). For any given value of H_o, the energy difference, ΔE , between the two spin states is

$$\Delta E = h\nu = g\beta H_o \tag{4}$$

If one irradiates a sample containing an unpaired electron in a magnetic field, with electromagnetic energy having a frequency ν, that satisfies Equation (4), electrons in the lower energy state absorb energy. If the system is at thermal equilibrium before irradiation, there will be a slightly larger number of electrons in the lower energy state than that in the higher energy state, and thus there will be a net absorption of energy from the radiation field. The measurement of this absorption, and of its variation as a function of wavelength forms the basis of ESR spectroscopy.

Under a given set of experimental conditions, the intensity of the ESR absorption is proportional to the number of unpaired spins in the sample. The **g** -value (determined by a measurement of the field H_o and the microwave frequency ν, at resonance) can supply useful information concerning the chemical nature of the species that contains the unpaired spin. The **g**-value is calculated as follow:

$$g = \frac{0.07145\nu}{10^{-4}H_0} \tag{5}$$

where the units of H_o are Gauss and ν is in GHZ

1.4 Organization

This work contains the results from two distinct studies. The first study was of organo-clays and is contained in chapter 2. The second study of AHA, including structure, metal ion coordination ability, and metal ion coordination mechanism of AHA is presented in chapter 3.

In chapter 2, we detail the synthesis of C_{16} nitrile -clay complexes, C_{16} amide-clay complexes, and the

4

hydrolysis of C_{16} nitrile on the clay interlayer surface. The interactions of coordination and dipole-ion occur between these nonionic modifiers and clay specific sites. Analysis of the peak shifts and the occurrence of new bands in the DRIFT spectra can be used to infer the interaction mechanisms and a model structure of organo-clay.[9, 10, 11] Specifically, the polar groups of the modifiers interact with the $Si^{\delta+}-O^{\delta-}-M^{n+}$ structure of montmorillonite clay to form a stable organo-clay through coordination and dipole-ion interaction which is lower sensitivity of electrolytes and solution pH. These properties are useful in the application of modified montmorillonite clay as a contaminant sorption material.

Chapter 3 describes the methods of structure analysis, metal ion interaction mechanisms, and metal ion coordination ability of AHA. Due to the complicated macromolecular characteristics of AHA, a deuteration method and a targeted reaction were used to aid in interpretation of the FTIR spectrum. Oxidation reaction of AHA by metal ions was used to investigate the characteristic structure of AHA and AHA-metal ion interaction mechanism. ESR spectra were used to detect semiquinone radical and metal species in the metal ion-AHA complexes which provide information about the metal ion-AHA interaction mechanism. The metal coordination ability of AHA was investigated under different solution pH. Because catechol represented a main reactive functional group of AHA,[12] we chose catechol as a model compound and investigated its metal coordination properties under the same conditions as that for AHA. The polymerization of catechol[13, 14] was reminiscent of the polymeric structure of AHA, which made catechol an acceptable model compound and give us better understanding of AHA.

Reference

1. Suffet, I. H.; MacCarthy, P. *Aquatic Humic Substances. Influence on Fate and Treatment of Pollutants* American Chemical Society, Washington, DC **1989**.

2. Murphy, E. M. ; Zachara, J. M. ; Smith, S. C. ; Phillips, J. L. *Sci. Total Environ.* **1992,** 413-423.

3. Grathwohl, P. *Environ. Sci. Technol.* **1990,** 24, 1687-1693.

4. Myers, D. *Surfactant Science and Technology* Second Edition VCH Publishers, Inc.New Yoek **1992.**

5. Cross, J. *Nonionic Surfactants Chemical Analysis* Marcel Dekker, Inc. New York **1987**.

6. Allard, B. ; Boren, H. ; Grimvail, A. *Humic substances in the Aquatic and Terrestrial Environment* **1989**, 357.

7. Colthup, N. B. ; Daly, L. H. ; Wiberley, S. E. *Introduction to Infrared and Raman Spectroscopy* Academic press, Inc. **1990**

8. Hayes, M. H. B.; MacCarthy, P.; Malcolm,R.L.; Swift, R. S. *Humic Substances II In Search of Structure* John Wiley & Sons New York. **1989.**

9. Isaacson, P. J. ; Sawhney, B. L. *Clay Miner.* **1982,** 18, 253.

10. Fusi, P. ; Ristori, G. G. ; Cecconi, S. ; Franci, M. *Clays Clay Miner.* **1983**, 26, 273.

11. Bowen, J. M.; Powers, C. R.; Ratcliffe, A. E. *Environ. Sci. Technol.* **1988,** 22, 1178-1181.

12. Stevenson, F. J. *Humus Chemistry* John Wiley & sons: New York, **1982**, 45.

13. Milorad, M. R. ; Timothy, R. D. *J. Am. Chem. Soc.* **1978**, 100:17, August 16, 5472.

14. Brubaker, C. H. Jr. ; Wicholas, M. *J. Inorg. Nucl. Chem.* **1965,** 27, 59.

CHAPTER II

DRIFT Study of Montmorillonite Clay Modification
by Nonionic Modifiers

Introduction

Natural clay is hydrophilic and cannot effectively absorb organic contaminants in groundwater systems. When a hydrophobic compound is used to modify the clay, the absorption ability for organic contaminants is effectively increased.[1] Many researchers have studied the partitioning of organic compounds onto natural clays [2, 3, 4] and organo-clays. [5, 6, 7, 8, 9, 10, 11]

Generally, the clay modifiers are surfactants containing distinct hydrophilic and hydrophobic groups. The existence of these two different moieties in the same molecule is responsible for the adsorption to the interlayer. Clay modifiers can be ionic and nonionic depending on the structure of hydrophilic parts. Compared with ionic modifiers, nonionic modifiers are low toxic and biodegradable. Furthermore, the modification process by nonionic modifiers is not as sensitive to electrolytes and solution pH. [12] Our research focused on the modification of montmorillonite clay by the nonionic modifiers heptadecanonitrile and hexadecanamide. We abbreviate these as C_{16} nitrile and C_{16} amide, respectively. Previous research has found that the C_{16} nitrile and C_{16} amide can be metabolized by bacteria to form completely nontoxic species. [13, 14] Therefore, the modification of montmorillonite clay by C_{16} nitrile and C_{16} amide does not create new environmental contaminants. Montmorillonite clay was chosen as a mineral fraction of typical soils because montmorillonite is common clay mineral and it has a large cation exchange capacity (CEC=80-150 meq / 100 grams). Furthermore, it has well-known composition and well-characterized structure. Some work has been published on the use of infrared (IR) spectroscopy for identifying active sites [15] and examining the interactions of adsorbates with them. [16]

In our research, we examined the interactions of organic modifiers C_{16} nitrile and C_{16} amide with montmorillonite clay at the molecular level using DRIFT spectroscopy. The structures of montmorillonite clay,[17] C_{16} nitrile, and C_{16} amide modifiers are given in Figure 2.1. Montmorillonite clay possesses strongly charged sites $Si^{\delta+}-O^{\delta-} M^{n+}$. The nonionic modifiers, C_{16} nitrile and C_{16} amide, have polar head groups which can interact with montmorillonite sites $Si^{\delta+}-O^{\delta-} M^{n+}$ through coordination and dipole-cation interactions to form organo-clay. DRIFT spectroscopy is the preferred method for the study compared to other infrared

7

techniques [18] due to its higher sensitivity for powders. The mechanisms of organo-clay interactions can be determined by analyzing the peak shifts and origins of the new bands in the DRIFT spectra. [19, 20, 21] In this study, we investigated the interactions between C_{16} nitrile modifiers and specific $Si^{\delta+}$-$O^{\delta-}$-M^{n+} site (s) and the influence of exchangeable metal cations on the interactions. We also studied the interactions between the C_{16} amide modifier and montmorillonite clay. Finally, we investigated the hydrolysis of C_{16} nitrile-clay complexes and the stability of these hydrolysis products. From this study, we could have a better understanding on the modification mechanisms of nonionic modifiers and their stability at different pH.
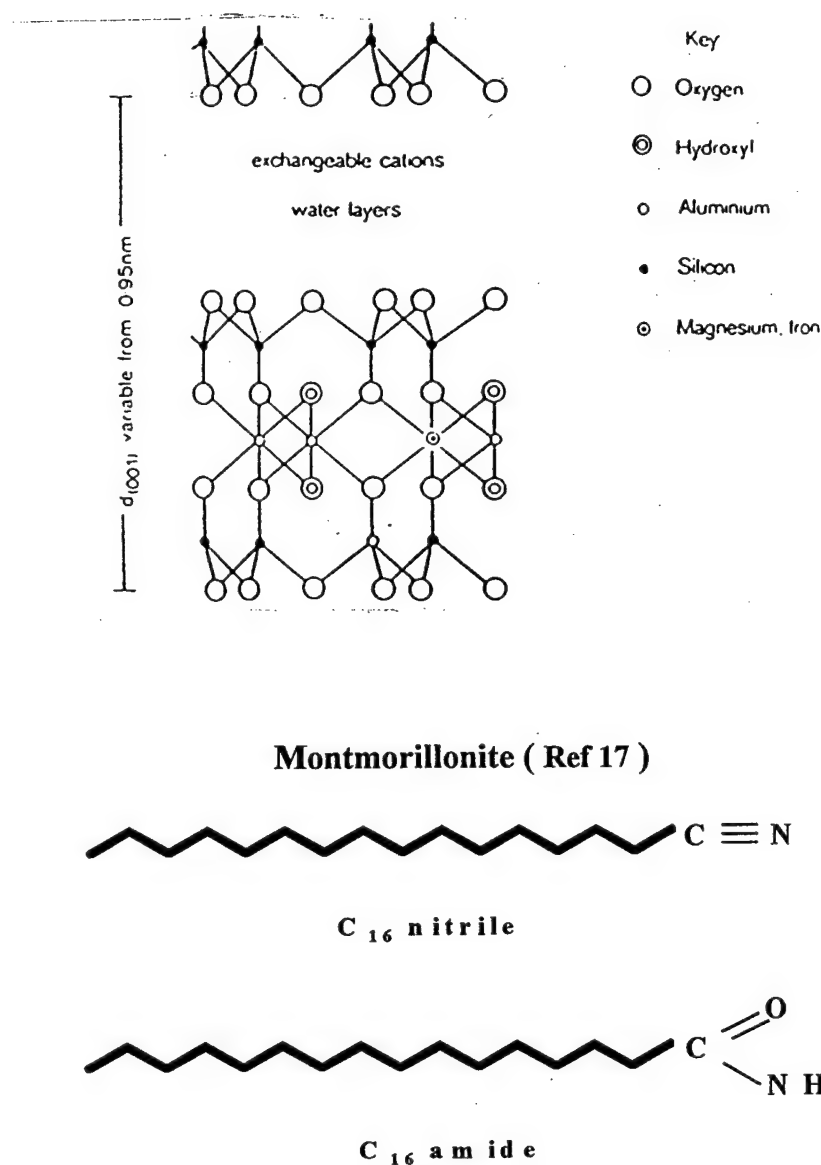
Figure 2.1. The structures of montmorillonite, C_{16} nitrile, and C_{16} amide

Experimental

2.1 Instruments

DRIFT spectra were taken with a Bomem 102 MB Series spectrometer. The background spectrum in this technique was obtained from KBr. Data was processed by Grams/ 386 software program. Spectra were recorded from 600-4000cm^{-1} with a resolution of 2 cm^{-1}. Sample powders for DRIFT spectra were mixed with KBr powder at 2-4% weight percent. The background spectrum of a pure KBr powder was automatically subtracted from the sample spectrum followed by an auto-baseline correction. A Praying Mantis Diffuse Reflection attachment was used for the DRIFT spectroscopy. The optical diagram of the Praying Mantis Diffuse Reflection attachment is shown in Figure 2.2.[22] The Praying Mantis design incorporates two 6:1 90° off-axis ellipsoidal mirrors, M3 and M4, which subtend 20% of the 2 pi solid angle. These mirrors are arranged with a common focal point, S. Mirrors M1 and M2 transfer the spectrometer beam to the first of these ellipsoids, M3. This mirror focuses the beam onto the sample, S. The second mirror collects the radiation diffusely reflected from the sample. This radiation is then directed by mirrors M5 and M6 toward the detector. The design of the Praying Mantis allows a high throughput and also has a large sampling space between the plate holders. In addition, the Praying Mantis discriminates against the collection of the specular component of the reflected beam.
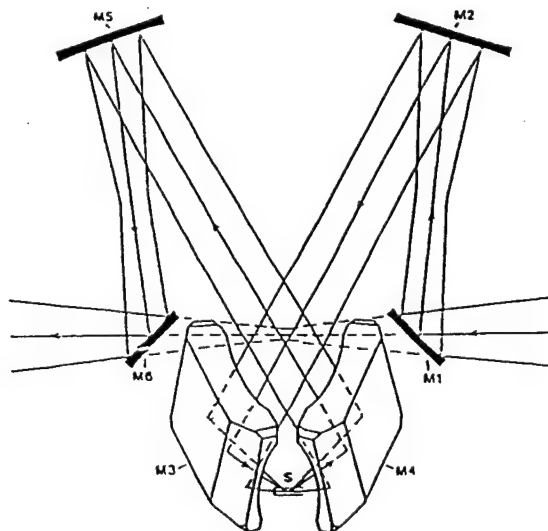
Figure 2.2 The optical diagram of the praying mantis diffuse reflection attachment

9

2.2 Preparation of the DRIFT Samples

The DRIFT samples were prepared as follows. Approximately 2 mg of the sample was mixed with 50mg of solid KBr and the mixture was ground into a fine powder. Approximately 25mg of this KBr-sample mixture was used to fill the sample compartment and a spectrum of the sample was obtained. The DRIFT spectrum of pure KBr powder was used as background.

2.3 Chemical Source

Montmorillonite was obtained from Aldrich (Iron saturated) and was purified by dispersing approximately two grams of the montmorillonite in about 200 ml of deionized water followed by vigorous agitation for about 30 minutes. The mixture was then allowed to settle, because larger particle impurities such as quartz sand and non colloidal minerals settle to the bottom of the mixture while the desired clay was suspended in the water. The clay suspension was then decanted, filtered, and dried in an oven at 100 °C.

The C_{16} nitrile and C_{16} amide were purchased from TCI America Company and were used without further treatment.

The cation exchange compounds trimethylammonium bromide (TAB), potassium perchlorate, sodium perchlorate, lithium perchlorate, copper(II) perchlorate, and manganese (II) perchlorate were purchased from Aldrich and were used as received. Absolute ethanol was purchased from Midwest Grain products of Pekin, Illinois and was used without further purification.

2.4 Synthesis

Synthesis of C_{16} nitrile-K^+montmorillonite Clay Complexes

Iron saturated montmorillonite clay was exchanged with the TAB and dried to give a TAB saturated montmorillonite clay (TAB-montmorillonite clay). Approximately two grams of the TAB-montmorillonite clay were refluxed with 50 ml of ethanol solution containing 0.16M potassium perchlorate and 0.16M C_{16} nitrile at 78° C for 48 hours. The sample was then washed with ethanol five times, centrifuged, and dried at 100° C for 24 hrs to give a C_{16} nitrile-K^+montmorillonite complexes.

Preparations of complexes of C_{16} nitrile with Na^+, Li^+, Ca^{2+}, Mn^{2+}, and Cu^{2+} saturated montmorillonite clay were identical to the method described above.

10

Synthesis of C_{16} amide-K^+ montmorillonite Complexes

Approximately two grams of the TAB-montmorillonite clay were refluxed with 50 ml of ethanol solution containing 0.16M potassium perchlorate and 0.16M C_{16} amide at 78° C for 48 hours. The sample was then washed with ethanol five times, centrifuged, and dried at 100° C for 24 hrs.

The Hydrolysis of C_{16} nitrile-K^+ montmorillonite Complexes

500mg of C_{16} nitrile-montmorillonite complexes and 10ml of 35% hydrochloric acid were placed in a 50mL three-necked round-bottomed flask equipped with glass joints. The flask was fitted with a reflux condenser, a thermometer, and a mechanical stirrer. The mixture was stirred vigorously at a bath temperature of about 40° C. During hydrolysis, the temperature of the reaction mixture rose about 10° C above that of the bath. The solution was kept in 40-50° C, stirring for 24hrs. The solution was cooled externally with ice water for about 30 minutes and centrifuged. The product was washed with 5% NaOH solution and centrifuged, followed by 5 washing with Millipore water. The final clean product was dried at 100°C for 24hrs. The DRIFT spectrum of the product was obtained by the same procedure as other samples.

Discussion

Formation Conditions and Stability of the C_{16} nitrile-M^{n+} montmorillonite Clay Complexes

It has been found that the formation of the C_{16} nitrile-M^{n+} montmorillonite clay complexes depends upon the montmorillonite clay characteristics and the solvent. When purchased the montmorillonite clay had been treated with $Fe(NO_3)_3$. We exchanged the metal cations of the montmorillonite clay with TAB cations to make it more hydrophobic. Once it is hydrophobic, it is easy for interlayer modification by C_{16} nitrile and C_{16} amide. These hydrophobic C_{16} nitrile-M^{n+} montmorillonite clay and C_{16} amide-M^{n+} montmorillonite clay are desirable for adsorption of organic contaminants in groundwater system. Ethanol is used as the solvent instead of the water because of the higher solubility of C_{16} nitrile and C_{16} amide in ethanol solvent. Figure 2.3 shows a scheme which represents a high-charge montmorillonite interacting with C_{16} nitrile and C_{16} amide to form hydrophobic C_{16} nitrile and C_{16} amide -montmorillonite clay.

Figure 2.4 shows the DRIFT spectra of pure C_{16} nitrile (2.4A), montmorillonite clay (2.4B), and C_{16} nitrile-montmorillonite complexes (2.4C). Figure 2.4A displays the free nitrile ($C \equiv N$) stretch at 2243 cm^{-1}. Upon interaction with the clay this peak shifts to 2249 cm^{-1} (2.4C).
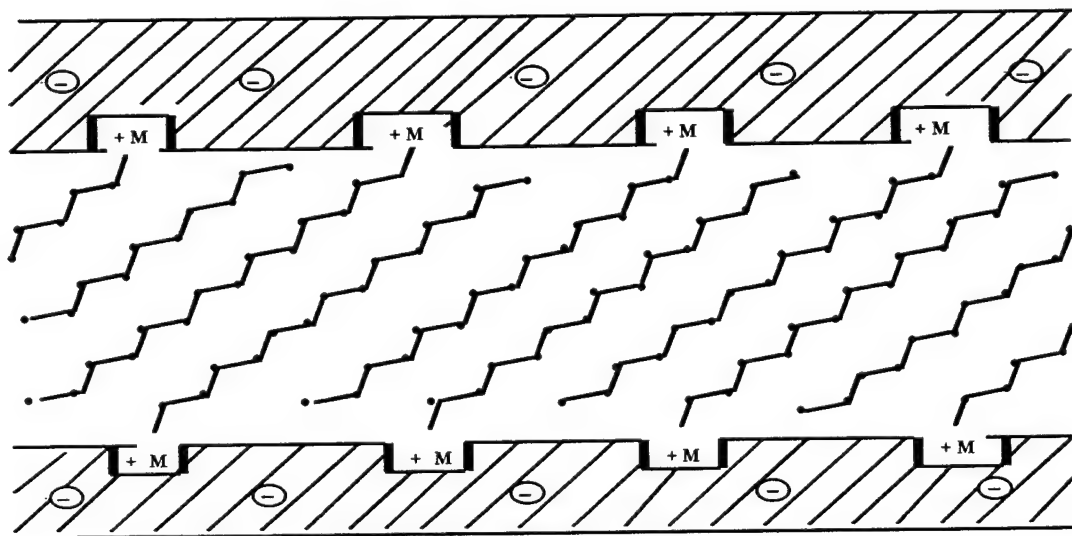
Figure 2.3 Interaction between nonionic modifiers and montmorillonite interface
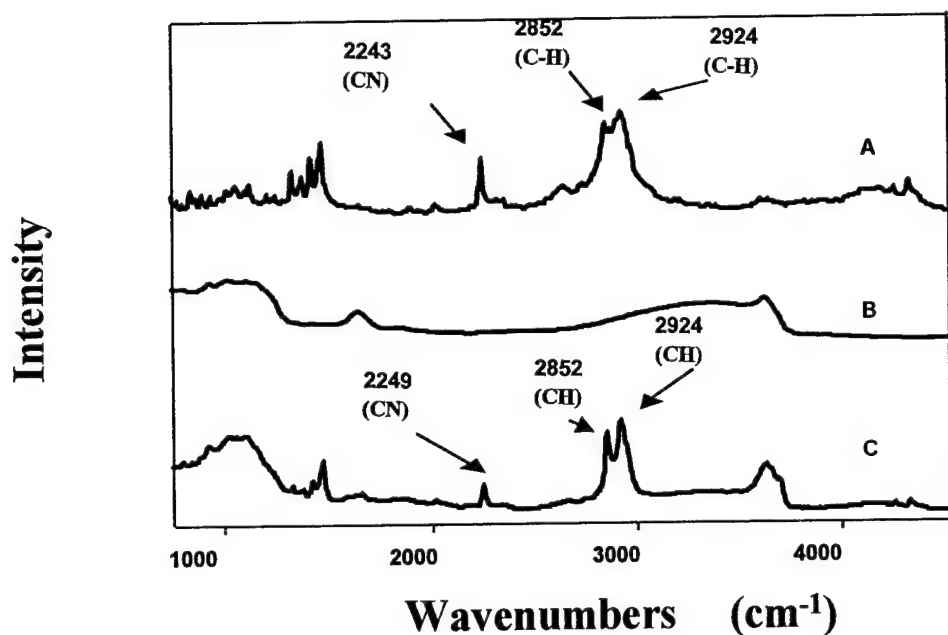
Figure 2.4 DRIFT spectra
A. Pure C$_{16}$ nitrile
B. Pure montmorillonite clay
C. C$_{16}$ nitrile-K$^+$montmorillonite clay complexes

The stability of the organo-clay was examined by washing of the organo-clay with water, 5% HCl, followed by 5% NaOH. It was found that washing produced no change in the C≡N stretch peak, which indicates that the organo-clay is quite stable and is not influenced by the normal solution's pH change.

Structure Analysis of C$_{16}$ nitrile -M^{n+}montmorillonite Clay Complexes

Dipole-Cation Interactions between the C≡N Structure and Interlayer Metal Cations

Our results showed that an interaction of C$_{16}$ nitrile and montmorillonite occurred between the nitrile C≡N structure and the interlayer cations of montmorillonite clay. The DRIFT band assignments [23,]

13

[24, 25] for pure C_{16} nitrile and C_{16} nitrile- K montmorillonite complexes are summarized in Table 2.1. The characteristic peaks of C_{16} nitrile are the C-H stretch at 2840-2930cm^{-1} regions and the C$\equiv$N stretch at 2243cm^{-1}, after interacting with K$^+$montmorillonite clay, the C$\equiv$N stretch undergoes a large frequency shift from 2243cm^{-1} to 2249cm^{-1} (Figure 2.4C).

Table 2.1 The DRIFT Band Assignments of C_{16} nitrile and C_{16} nitrile -K$^+$ Montmorillonite Complexes

DRIFT band assignments	C_{16} nitrile (cm^{-1})	C_{16} nitrile on K$^+$montmorillonite clay surfaces (cm^{-1})	C_{16} nitrile on Cu^{2+} montmorillonite clay surfaces (cm^{-1})
C$\equiv$N	2243.6	2249	2248-2301
CH$_2$ symmetric stretch	2851.3	2852.5	2849.8
CH$_2$ asymmetric stretch	2923.6	2924.9	2920.4

Farmer [26] suggested that the magnitude of the spectral shift should be dependent on the types of the cations when the interaction of the modifiers with the cations is C$\equiv$N-metal ion interaction. In this study, we synthesized six different kinds of C_{16} nitrile-M^{n+}montmorillonite complexes each was saturated with different metal ion: Li$^+$, Na$^+$, K$^+$, Ca^{2+}, Cu^{2+}, or Mn^{2+}. It is found that the nitrile C$\equiv$N bond shifts changed with the metal ions. In Li$^+$, Na$^+$, and K$^+$ saturated montmorillonite, the shifts are about 6-9cm^{-1} (Figure 2.5). In Ca^{2+}, Cu^{2+}, and Mn^{2+} saturated montmorillonite the shifts are as large as 26 cm^{-1} for C_{16} nitrile-Ca^{2+} montmorillonite complexes (Figure 2.6A), 30 cm^{-1} for C_{16}nitrile-Mn^{2+}montmorillonite complexes (Figure 2.6B), and 58 cm^{-1} for C_{16} nitrile-Cu^{2+}montmorillonite complexes (Figure 2.6C). Since the divalent metals produce a larger shift, it can be concluded that the interactions between C_{16} nitrile and clay interface is a dipole-ion interaction between C$\equiv$N and interlayer metal ions.
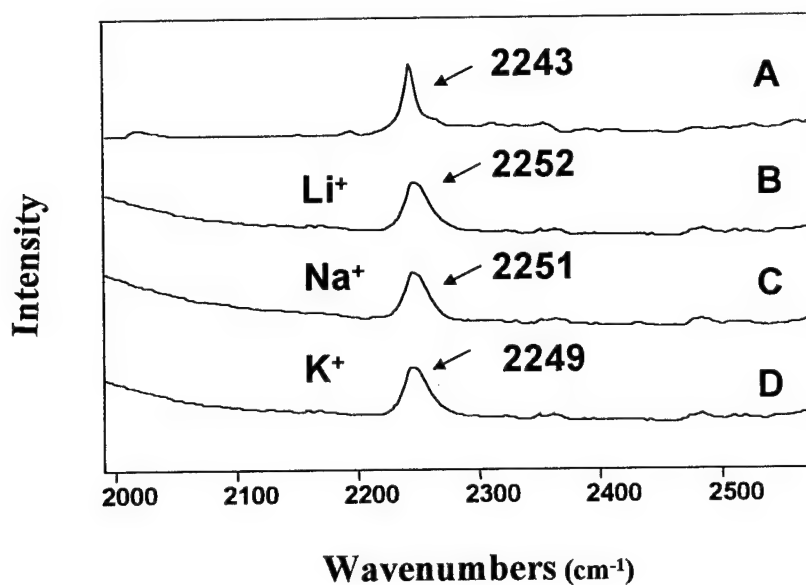
Figure 2.5 The nitrile stretch band shift
A. Pure C $_{16}$nitrile
B. C $_{16}$nitrile - Li $^+$Montmorillonite clay
C. C $_{16}$nitrile - Na $^+$Montmorillonite clay
D. C $_{16}$nitrile - K $^+$Montmorillonite clay
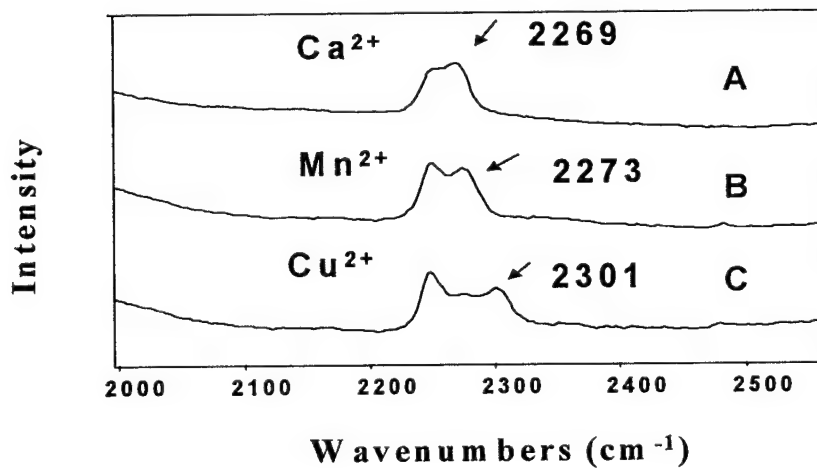
Figure 2.6 The nitrile stretch band shift
A. C $_{16}$nitrile - Ca $^{2+}$ Montmorillonite clay
B. C $_{16}$nitrile - Mn $^{2+}$Montmorillonite clay
C. C $_{16}$nitrile - Cu $^{2+}$ Montmorillonite clay

Newman [27] found that the dipole-ion interaction should be proportional to the ratio of Z/r of metal ions, where Z is the charge and r is the ionic radius. We plot the C≡N band shifts with the ratio of Z/r of metal ions (Figure 2.7). The plot is not linear. A noticeably larger C≡N band shift was observed for C_{16} nitrile-Cu^{2+} montmorillonite complexes. This indicates that the interaction mechanism between the C≡N and Cu^{2+} may be different. For example, Cu^{2+} has unoccupied d-orbitals, and N has lone pair electrons which can transfer to the unoccupied d-orbitals of Cu^{2+} to form a coordination bond which will give a larger C≡N band shift.
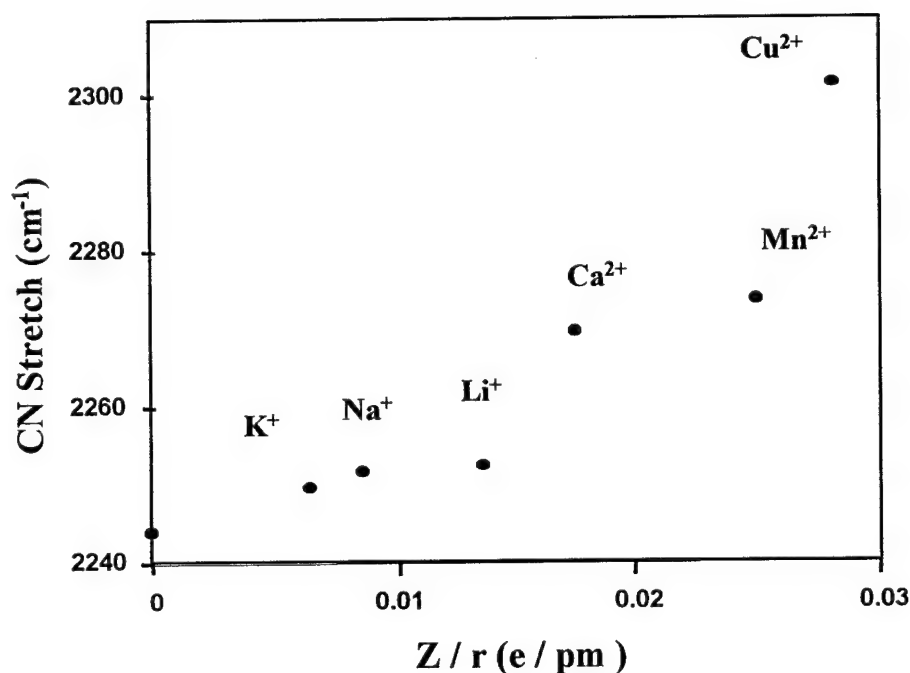
Figure 2.7 The plot of C≡N stretch - charge Z / radii r of metal ions

The model structure of C_{16} nitrile-Cu^{2+} montmorillonite clay complex is shown in Figure 2.8.

The strengthening of C≡N bond during the coordination or dipole-ion interaction process can be explained by the bond order theory of coordination chemistry.[28] The lone pair electrons on the N of C≡N functional groups reside in a molecular orbital that is slightly anti-bonding. When these lone pair electrons

16

transferred or shifted from the original orbital, the bond order of $C\equiv N$ will slightly increase, resulting in the increase of stretching frequency of $C\equiv N$.
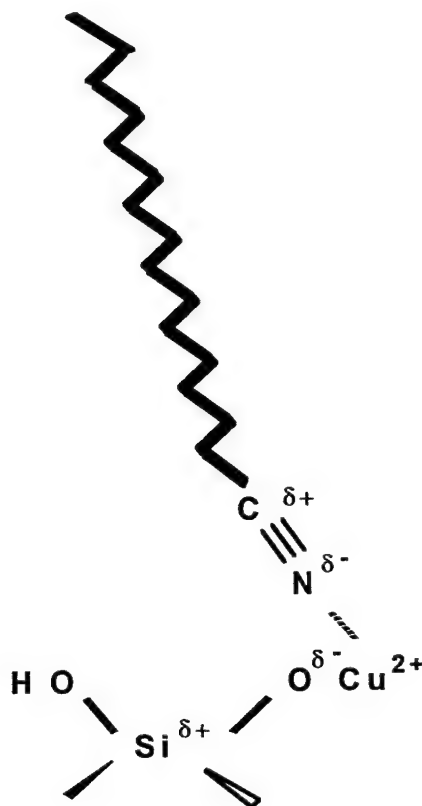
Figure 2.8 The model structure of C_{16} nitrile - Cu^{2+}montmorillonite clay complexes

The $N^{\delta-}-M^{n+}$ dipole-cation interaction between modifier C_{16} nitrile and the montmorillonite clay results in stable complexes. The stability of organo-clay is demonstrated by the resistance to the stronger ionic concentration and normal pH changes. This property is desirable in the possible application of this modified clay as a wastewater treatment agent.

Structure Analysis of C_{16} amide -K^+montmorillonite Clay Complexes

C16 amide was chosen as another possible nonionic modifier. The long chain and biological nontoxicity make it popular as a surfactant. A study of coordination between C16 amide and montmorillonite clay could help us better understand the possible hydrolysis of C16 nitrile modifier on the montmorillonite clay. Figure 2.9 is the DRIFT
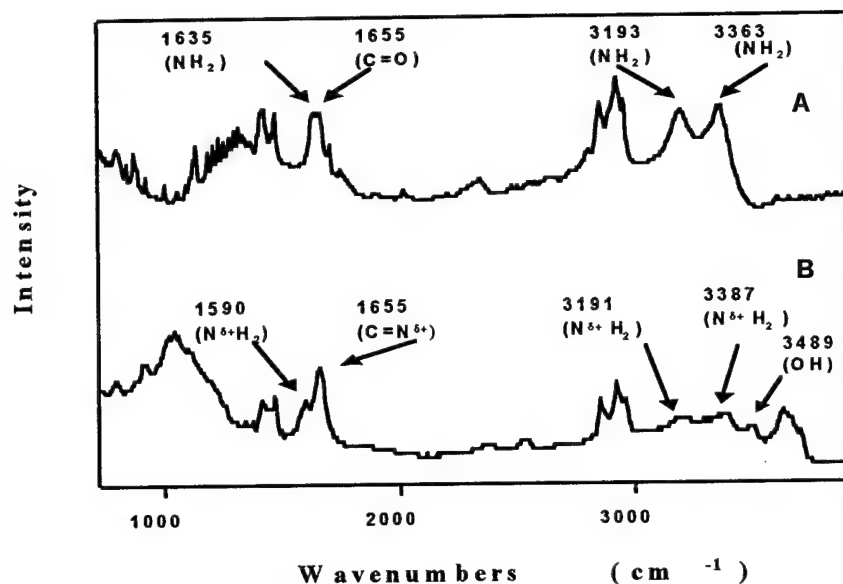
Figure 2.9 DRIFT spectra
A. C16 amide
B. C16 amide-K+ montmorillonite clay complexes

spectra of the pure C_{16} amide (2.9A) and C_{16} amide-K+montmorillonite complexes (2.9B). The peak assignments are listed in Table 2.2. The C=O stretch, NH_2 stretch, and NH_2 deformation peaks all shifted after the formation of the C_{16} amide-K+ montmorillonite clay complexes. Other researchers [23] found that the amide group has a large contribution from the resonance structure, $^{-\delta}$O-C=N$^{\delta+}H_2$. This resonance structure is formed by the weakening of the C=O bond and increasing of the C-N bond strength of O=C-NH_2 (Figure 2.10). For an amide resonance structure, the C=N$^{\delta+}$ stretch vibration should appear in the 1630-1690 cm^{-1} region and the N$^{\delta+}H_2$ deformation should appear in the 1560-1620 cm^{-1} region. [23, 24]

$$\text{R-C-NH}_2 \longleftrightarrow \text{R-C=N}^{\delta+}\text{H}_2$$
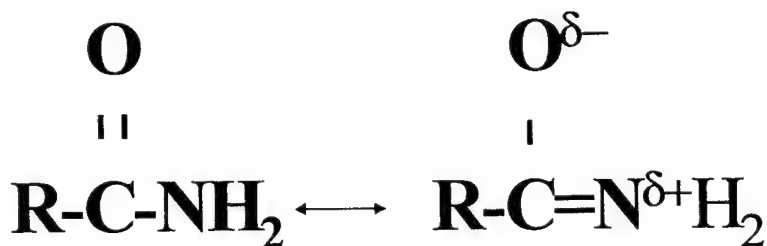
Figure 2.10 The resonance structure of C_{16} amide

18

We found that C_{16} amide exists as its resonance structure on the montmorillonite clay interface as evidenced by the DRIFT spectrum of C_{16} amide-montmorillonite complexes (2.9B). The resonance structure could be induced by the specific Si $^{\delta+}$-O $^{\delta-}$-M^{n+} structure of montmorillonite clay. The spectrum (2.9B) shows peaks at 1655 cm^{-1} and 1590 cm^{-1} regions which could be reasonably identified as the C=N$^{\delta+}$ stretch and N$^{\delta+}$H$_2$ deformation, respectively. [23, 25] The peaks at 3191cm^{-1} and 3387cm^{-1} (2.9B) could be identified as the asymmetric and symmetric NH$_2$ stretch. A new peak at 3489cm^{-1} (2.9B) could be due to the hydrogen bonding formed between N-H functional groups and Si$^{\delta+}$ –O$^{\delta-}$ sites and between C-O$^-$ functional groups and Si$^{\delta+}$ –OH sites of clay interface.

The model structure of C_{16} amide-K$^+$montmorillonite clay surface complex is shown in Figure 2.11. The ring structure formed between the modifier and montmorillonite clay plays an important role in the stabilization of the C_{16} amide-K$^+$montmorillonite clay complexes.
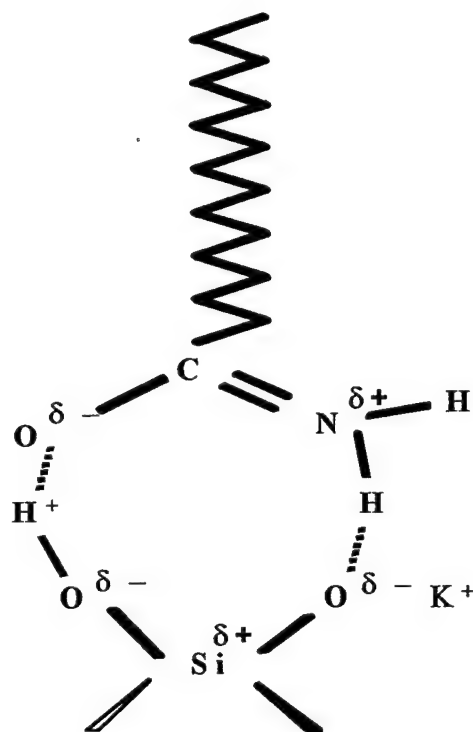
Figure 2.11 The model structure of the C_{16} amide-K$^+$montmorillonite clay complex

Table 2.2 The DRIFT Band Assignments of C_{16} amide and C_{16} amide-K^+montmorillonite Complexes

peak assignments	C_{16} amide (cm^{-1})	C_{16} amide- K^+montmorillonite complexes (cm^{-1}) (resonance structure of C_{16} amide)
C=O stretch	1655	
NH_2 deformation	1635	
$C=N^{\delta+}$ stretch		1655
$N^{\delta+}H_2$ deformation		1590
NH_2 symmetric stretch	3193	3191
NH_2 asymmetric stretch	3363	3387
OH bond		3489

The Hydrolysis of C_{16} nitrile -K^+ montmorillonite Complexes

Wade, jr. [29] and Cross [30] showed that the C_{16} nitrile can be hydrolyzed to form C_{16} amide. In this study, we examined the hydrolysis of the C_{16} nitrile-K^+montmorillonite clay complexes to better understand the behavior of organo-clay. The DRIFT spectrum of the hydrolyzed product of C_{16} nitrile- K^+montmorillonite complex is shown in Figure 2.12B. It was found that, after the hydrolysis, the nitrile C≡N peak at 2249 cm^{-1} disappeared. The new peaks which appeared at 1655 cm^{-1}, 1590 cm^{-1}, and 3387 cm^{-1} are indicative of the $C=N^{\delta+}$ bond stretch, $N^{\delta+} H_2$ deformation, and the asymmetric NH_2 stretch [23, 25] of amide resonance structure, respectively. The peak at 3489cm^{-1} can be OH bonding between amide and montmorillonite. To further study the structure of the hydrolysis product of C_{16} nitrile-K^+montmorillonite complex we compared the DRIFT spectrum of hydrolyzed C_{16} nitrile-K^+montmorillonite complex with that of the C_{16} amide-K^+montmorillonite complex. It was found that they are identical (Figure 2.12 B and C). Therefore, it is apparent that the C_{16} nitrile-K^+montmorillonite complexes can be hydrolyzed to form C_{16} amide-montmorillonite complexes. Figure 2.13 shows the hydrolysis reaction of C_{16} nitrile on a montmorillonite interface.

The peak assignments of hydrolyzed C_{16} nitrile-K^+montmorillonite clay complexes are the same as that of C_{16} amide-K^+montmorillonite clay complexes, both exist as the amide resonance structure.   The

interactions between $O^{\delta-}-C=N^{\delta+}H_2$ and $Si^{\delta+}-O^{\delta-}-M^{n+}$ structure create a ring structure which makes the hydrolyzed C_{16} nitrile-montmorillonite complexes stable even at strong acidic condition (35% HCl solution). Figure 2.14 shows the hydrolysis mechanism.

A . C_{16} nitrile-K^+ montmorillonite complexes
B . Hydrolyzed C_{16} nitrile-K^+ montmorillonite complexes
C . C_{16} amide-K^+ montmorillonite complexes
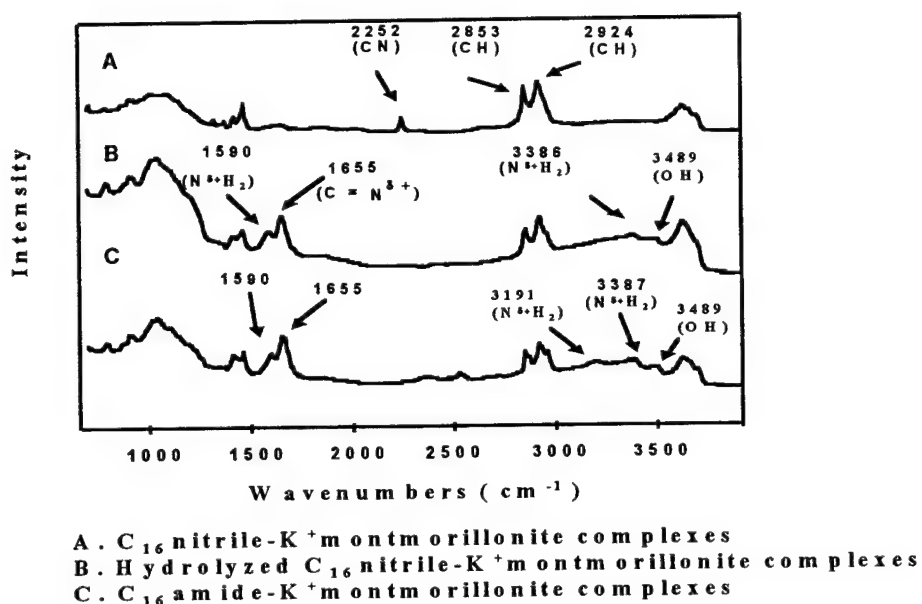
Figure 2.12 DRIFT Spectra
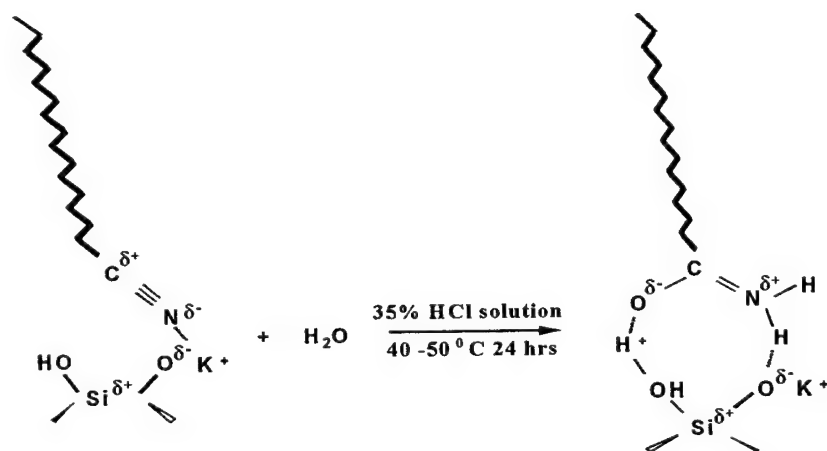
Figure 2.13 Hydrolysis reaction of C_{16} nitrile on montmorillonite interface

21

$$R\text{-}C \equiv N: \ + \ H^+ \ \xrightarrow{\text{Protonation}} \ R\text{-}C \equiv N^+H \longrightarrow$$
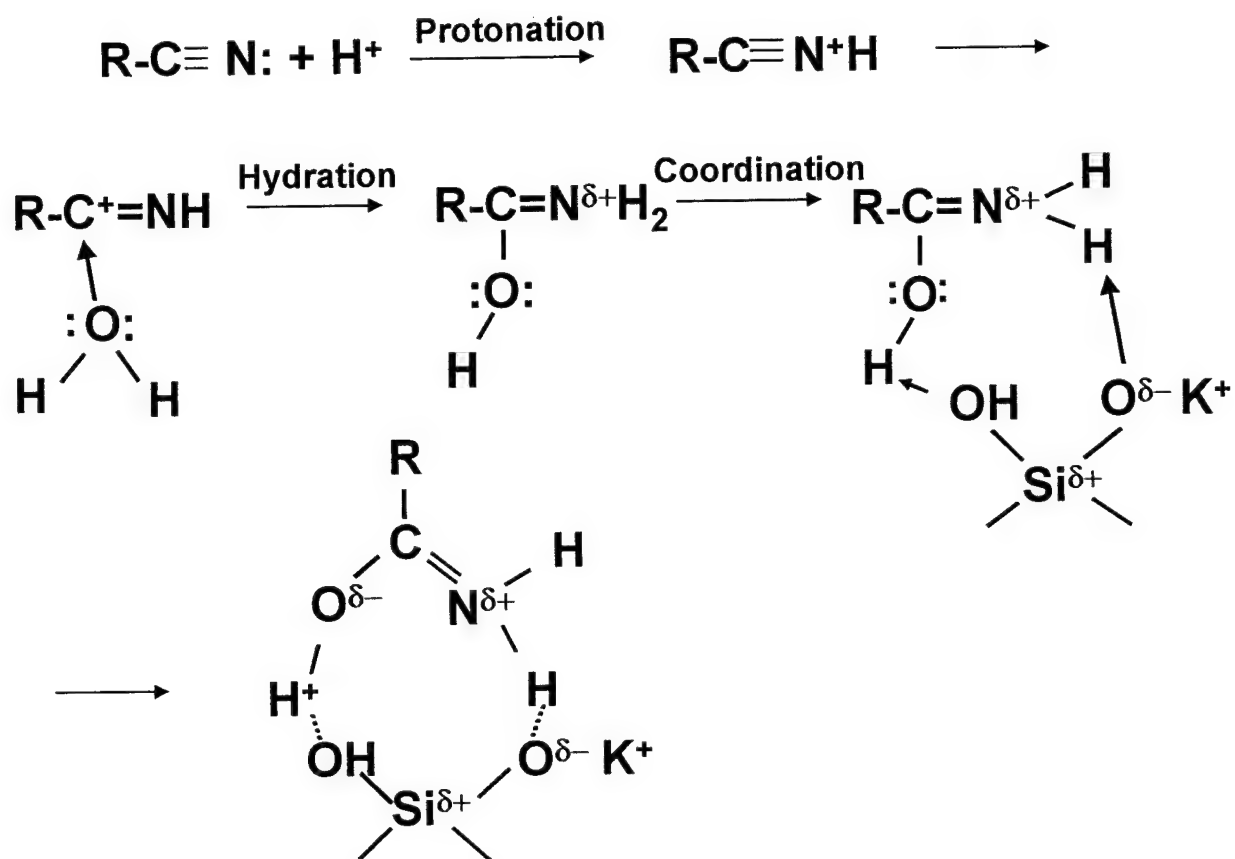
Figure 2.14 Hydrolysis mechanism of C_{16} nitrile

22

Conclusion

It has been shown that the specific interactions between C_{16} nitrile and montmorillonite clay can be determined by using DRIFT techniques. An analysis of the spectral shifts of the C_{16} nitrile vibrational bands after the modification indicates that the major interaction between montmorillonite clay and the C_{16} nitrile molecule is dipole-cation interaction. In the case of the transition metal cation Cu^{2+}, a coordination bond can be formed. The investigation of montmorillonite clay modified by C_{16} amide indicates that C_{16} amide existed predominantly as a resonance structure due to induction by $Si^{\delta+}-O^{\delta-}-M^{n+}$ sites of montmorillonite clay. Two interactions between C_{16} amide and montmorillonite clay and formation of a stable ring structure account for the stability of the amide on the clay.

Under strong acidic conditions, C_{16} nitrile-K^+montmorillonite complexes can be hydrolyzed to form a C_{16} amide-K^+montmorillonite adduct. The hydrolyzed C_{16} nitrile also existed predominantly as a resonance structure of C_{16} amide. The interaction mechanisms between hydrolyzed C_{16} nitrile and montmorillonite clay are identical to that between C_{16} amide and montmorillonite clay.

The montmorillonite clay modification by nonionic modifiers C_{16} amide and C_{16} nitrile are stable at 5% acidic and basic concentration. The hydrolysis of C_{16} nitrile on the montmorillonite clay at strong acidic condition is a transfer process from C_{16} nitrile to C_{16} amide, which also forms a stable ring structure. This property is desirable in the possible application of this modified clay as a wastewater treatment agent. In addition, nonionic modifiers C_{16} nitrile and C_{16} amide are biodegradable and harmless for micro-organisms in aqueous media. Therefore, the use of the C_{16} nitrile and C_{16} amide as clay modifiers does not create new environmental contaminants.

Reference

1. Jaynes, W. F.; Vance, G. F. *Soil Sci. Soc. Am. J.* **1996,** 60, 1742-1749.

2. Johnson, R. L.; Cherry, J. A.; Pankow, J. F. *Environ. Sci. Technol.* **1989**, 23, 340.

3. Subramanian, P.; Fitch, A. *Environ. Sci. Technol.* **1992,** 26, 1775.

4. Wang, X. O.; Thibodeaux, L. J.; Valsarj, K. T.; Reible, D. D. *Environ. Sci. Technol.* **1991,** 25, 1578.

5. Boyd, S. A.; Mortland, M. M.; Chiou, C. T. *Soil Sci. Soc. Am. J.* **1988**, 52, 652.

6. Boyd, S. A.; Shaobai, S.; Lee, J. F.; Mortland, M. M. *Clays Clay Miner.* **1988,** 36,125.

7. Jaynes, W. F.; Boyd, S. A. *Soil Sci. Soc. Am. J.* **1991**, 55, 43.

8. Lee, J.; Crum, J. R.; Boyd, S. A. *Environ. Sci. Technol.* **1989**, 23, 1365.

9. Faschan, A.; Tittlebaum, M.; Cartledge, F. *Haz. Waste. Waz. Mat.* **1993,** 10, 313.

10. Srinivasan, K. R.; Fogler, H. S. *Clays Clay Miner.* **1990**, 38, 277.

11. Srinivasan, K. R.; Fogler, H. S. *Clays Clay Miner.* **1990**, 38, 287.

12. Myers, D. *Surfactant Science and Technology* Second Edition, VCH Publisher, Inc.**1992**

13. Steen, W. C. ; Collette, T. W. *Applied Environmental Microbiology* **1989**, 55, 2545-2549.

14. Aislabie, J.; Atlas, R. M. *Applied Environmental Microbiology* **1988**, 54, 2197-2202.

15. Knozinger, H.; Ratnasamy, P. *Catal. Rev. Sci. Eng.* **1978**, 17, 31.

16. Kung, M. C.; Kung, H. H. *Catal. Rev. Sci. Eng.***1985**, 27, 425.

17. Theng, B. K. G. *Formation and Properties of Clay-Polymer Complexes* Developments in soil science; V9. Elsevier Scientific Publishing Company. **1979**

18. Bowen, J. M.; Compton, S. V.; Blanche, M. S. *Anal. Chem.* **1989**, 61, 2047-2050.

19. Isaacson, P. J.; Sawhney, B. L. *Clay Miner.* **1982**, 18, 253.

20. Fusi, P.; Ristori, G. G.; Cecconi, S.; Franci, M. *Clays Clay Miner.* **1983,** 26, 273.

21. Bowen, J. M.; Powers, C. R.; Ratcliffe, A. E. *Environ. Sci. Technol.* **1988,** 22, 1178-1181.

22. Bomem, Inc. *The Michelson Series User's Guide.* Version 1.0, **1994.**

23. Colthup, N.B.; Daly, L.H.; Wiberley, S.E. *Introduction to Infrared and Ramam Spectroscopy.* Third Edition. **1990,** 418-469.

24. Nakamoto, K. *Infrared Spectra of Inorganic and Coordination Compounds* Second Edition. John Wiley

& Sons, Inc. New York, **1970.**

25. Bellamy, L. J. *The Infrared Spectra of Complex Molecules* John Wiley & Sons, Inc.New York, **1957**

26. Farmer, V. C. *Soil Sci.* **1971,**112,62.

27. Newman, A.C.D. *Chemistry of Clays and Clay Minerals* John Wiley & Sons. **1987**

28. Huheey, J. E.; Keiter, E. A.; Kerter, R. L. *Inorganic Chemistry* Fourth Edition. Harper Collins College Publishers. **1993**

29. Wade, jr. L.G. *Organic Chemistry* Prentice Hall, Englewood Cliffs, NJ. **1987.**

30. Cross, J. *Nonionic Surfactants* Marcel Dekker, Inc. New York, **1987**

CHAPTER III

Transmittance Infrared Spectra Study of Humic Acids: Catechol as a Model Compound

Introduction

Interactions of hazardous waste materials with dissolved natural humic substances can significantly influence the transport and fate of the compounds in aquatic systems. Hazardous waste materials include a wide variety of species. Concerning the interaction with HA the most important of these species include organohalides, polycyclic aromatic hydrocarbon, heavy metal ions, reducible metal ions, soluble oxidants, iron compounds, aluminum compounds, strong acids, and bases.[1] Caron and Suffet [2] have shown that the transport, reactivity, and fate of hydrophobic organic contaminants are affected by the nature of the compounds and the HA. Hart et al.[3] found that the HA can act as chelating agents for metal ions, including heavy metal ions and reducible metal ions. Szilagyi [4] indicated that HA is an active oxidation-reduction system. HA can influence the oxidation-reduction of metal species by stabilizing the reduced cationic forms by chelation, for example, the unchelatable oxoanion $Cr_2O_7^{2-}$ can be reduced by HA to chelatable cationic Cr^{3+}.[1]

Extensive research [5, 6, 7] indicated that the sorption and interaction of inorganic and organic contaminants to HA is influenced by the chemical properties of the HA. Kim et al. [1] have investigated and characterized HA by elemental analysis, acidic functional group analysis, and apparent-molecular-weight (AMW) distribution analysis (Table 3.1). A model molecular structure for HA has been proposed by Stevenson (Figure 3.1),[8] who proposed that the functional structures of HA are mainly catechol and phthalic acid analogues.

Although previous research has found that the reducible metal cations can interact with HA by reduction-chelation, the influence of reducible metal cations Fe^{3+} and Cu^{2+} (common or hazardous metal ions in the subsurface system) on the HA structure is not known yet. Pierpont and Lange [9] have studied the chemistry of Cu^{2+} and Fe^{3+} -organo complexes. They found that the Cu^{2+} and Fe^{3+} have a strong affinity to hard O-donor ligands, and more specifically for the catechol ligand. The catechol ligand

Table 3.1 Characterization of Aldrich Humic Acids (AHA)

Elemental analysis %					AMW* distribution by Ultrafiltration (%)		Acidic functional group analysis(meq/g)	
C	H	N	O	Ash	>50,000	10,000<MW<50,000	COOH	Phenolic OH
51.5	4.8	0.8	43.0	9.4	94%	6%	3.3	2.5

* AMW is apparent-molecular-weight

is an important functional group of HA [8] and is uniquely suited for iron and copper cation coordination. An example of the strong binding can be seen from the very large formation constant of 10^{49} of tris (catecholato) iron(III) complex anion. [9] Cu^{2+} cations can also coordinate catechol to form bridge dimer complexes. [9] They further proposed that a strong catechol to Cu^{2+} and Fe^{3+} metal cation charge transfer (LMCT) would result in semiquinone character for the coordinated catecholate ligand. Milorad et al. [10] and Brubaker et al. [11] indicated that the catechol structure can be oxidized and further polymerized to form polymers by reducible metal cations such as Cu^{2+} and Fe^{3+}. Previous researchers [12,13,14,15] also found that the coordination between metal cations and HA can be influenced by the configuration of dissolved HA, which is in turn affected by pH, ionic concentration, and electrolyte cations. Based on these observations, we believe that studies of the structure of AHA, the influence of reducible metal cation on the structure, and their interaction mechanisms at different pH and temperature conditions will contribute greatly to the understanding of natural HA chemistry in subsurface systems. We use AHA as a representative of natural HA due to cost and availability considerations.

The principal goals of this study are: (1) to characterize and simulate the functional groups of the AHA, (2) to find an appropriate model compound for AHA, and (3) to elucidate Cu^{2+} and Fe^{3+} coordination mechanisms and coordination abilities of the AHA and the model compounds. In this work, the study of the structure and functional groups of AHA was determined by FTIR spectroscopy, deuteration, and redox reaction. The study of the metal coordinating abilities and the interaction mechanisms of AHA and catechol model compound was determined by elemental analysis, FTIR spectra, and ESR spectra. Elemental analysis was also used to model the molecular structures of Cu^{2+} and Fe^{3+}-catechol complexes. Finally, we elucidated the similarity between model catechol- metal complexes and AHA -metal complexes by their structures, their coordination site selectivity, their bonding mechanisms, and their coordination abilities.
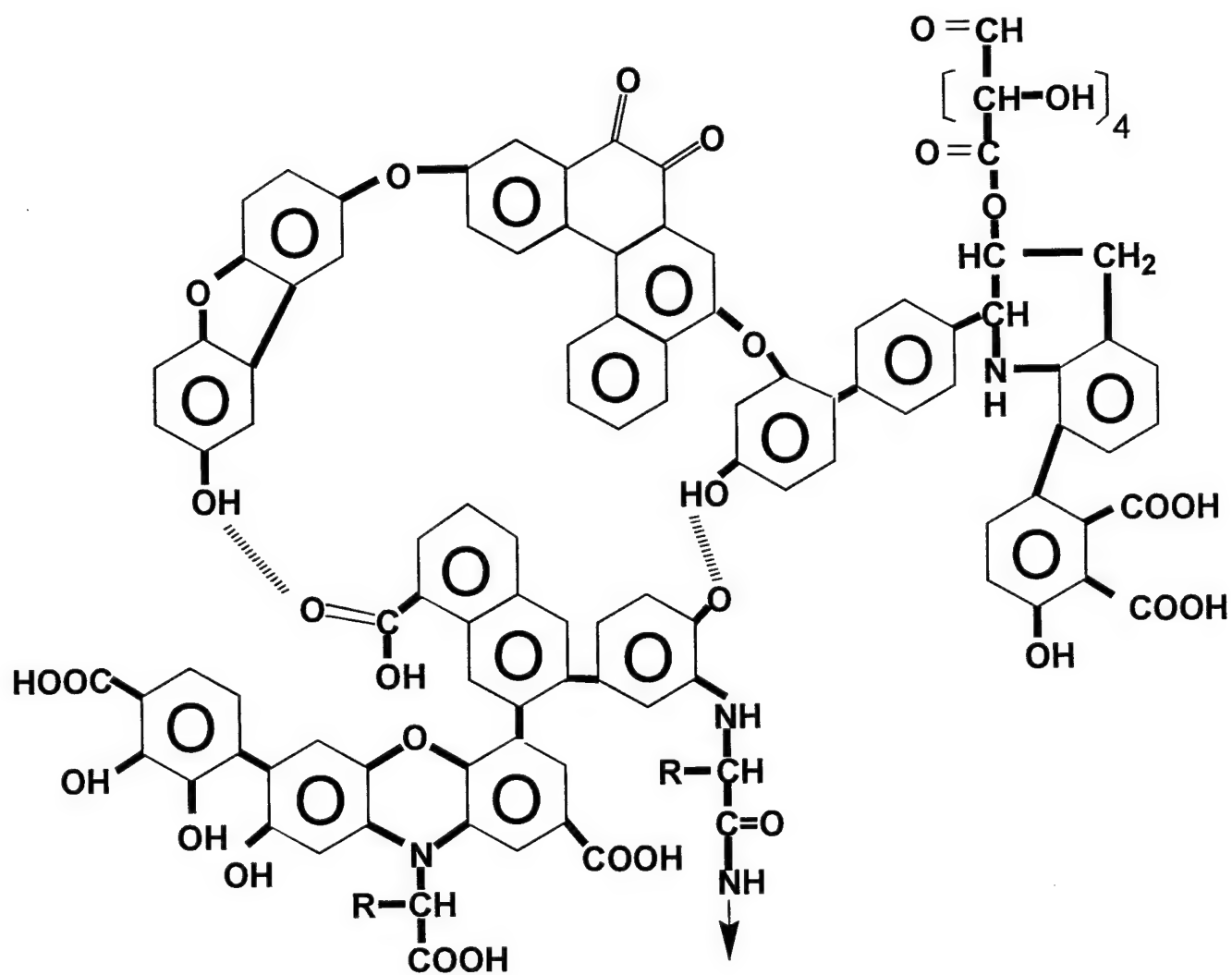
27

Figure 3.1 The model structure of AHA (proposed by Stevenson)

28

Experimental

I. Instrumental

Transmission FTIR spectra were taken by a Bomem 101MB Series spectrometer and data was processed by the Grams/ 386 software. Spectra were recorded from 600-4000 cm^{-1} with a resolution of 2 cm^{-1}. Samples were made up in KBr pellets at 2-4% concentration. The background of a pure KBr pellet was automatically subtracted from the spectra followed by an auto-baseline correction.

CHNS analysis was performed using an Ea1108 CHNS elemental analyzer (Fisons Instruments). Data manipulations were performed using Eager 200 computer programs. The analysis for Cu^{2+} and Fe^{3+} was done on a PE372 Perkin- Elmer atomic absorption spectrophotometer. The chloride analysis was done by the Atlantic Micro Lab.

ESR spectra were generated on a Varian E-3 X band spectrometer. DMSO was used as the solvent for sample preparation (15mg sample / 2ml DMSO).

II. Materials

AHA was obtained from Aldrich and was purified by washing with deionized water solution acidified with HCl to pH 2. The relative functional group distribution (COOH and OH) in the AHA was estimated to be about 5.8mmoles of functional groups / gram AHA (Table 3.1). Catechol (Eastman Kodak Company, assay 98%), cupric chloride and sodium hydroxide pellets (J. T. Baker Chemical Co. assay 100.8% and 98.7%, respectively), ferric chloride (Mallinckrodt, Inc. assay 98%), DMSO (Fisher Scientific, assay 99.7%), and copper (II) acetate mono-hydrate (Aldrich, assay 98%) were used as received.

III. Complex Synthesis

Synthesis of Cu^{2+}, Fe^{3+} -AHA Complexes

In order to investigate the influence of solution pH and temperature on metal coordination by AHA,

29

we made the Fe^{3+} and Cu^{2+}-AHA complexes at the following conditions: pH=1 at 60-70° C temperature (condition I); pH=1 at room temperature (condition II); pH=6 or 7 at room temperature (condition III).

The Cu^{2+} and Fe^{3+}-AHA complexes at condition I and II were made by mixing 1.515g of the AHA in 80 mL H_2O with 10 mL of 2M $CuCl_2$ or $FeCl_3$ aqueous solutions at 60-70° C or at room temperature for 24 to 72 hrs. The ratio of COOH and OH functional groups to Cu^{2+} & Fe^{3+} was about 1mole : 2.28moles. solution pH was adjusted to 1 by addition of HCl. The final products of both the Cu^{2+}-AHA complexes and Fe^{3+}-AHA complexes were washed with HCl deionized water (pH=1), centrifuged, and freeze dried for 24 hrs. The final product was brown. The concentration of Cu^{2+} or Fe^{3+} in the metal-AHA complexes are shown in Table 3.2.

The Cu^{2+}-AHA complexes at the condition III were made by mixing 2.5863g of AHA in 70 mL water with 30mL of 0.36M $Cu(OAc)_2$ (pH=6) at room temperature for 72 hrs. The ratio of COOH and OH functional groups to Cu^{2+} = 1mole : 0.72moles. The Fe^{3+}-AHA complexes were made by mixing 2.4827g AHA in 100mL H_2O with 720 mL of 0.002M $Fe(OH)_3$ aqueous slurry (pH=7) at room temperature for 72 hrs, where the ratio of COOH and OH functional groups to Fe^{3+} was made to be 10moles : 1mole. The final products of both Cu^{2+}-AHA complexes and Fe^{3+}-AHA complexes were washed with deionized water, centrifuged, and freeze dried for 24 hrs, also resulting in a brown powder.

Table 3.2 The Concentration of Cu^{2+} and Fe^{3+} in the Metal-AHA Complexes

reaction conditions	Cu^{2+} % in metal-catechol complexes	Cu^{2+} % in metal-AHA complexes	Fe^{3+} % in metal-catechol complexes	Fe^{3+} % in metal-AHA complexes
condition I	3.51	2.73	6.91	8.79
condition II	13.96	8.52	4.45	2.65
condition III	21.92	13.13	16.40	12.96

Deuteration

Pure AHA, catechol, phthalic acid, and their Cu^{2+} and Fe^{3+} complexes were deuterated by exchanging the H with D using D_2O at temperatures of 90-100° C for 1-3 days. The final products were isolated by centrifuging and freeze drying the mixture overnight.

Synthesis of Isopropylammnium Humate

In order to identify the C=O functional group of quinone from the C=O structure of carboxylic acid of AHA we used isopropylamine to have a targeted chemical reaction. Carboxylic acid group of AHA can react with isopropylamine to form isopropylammonium humate, which shows significantly different FTIR characteristic peaks. D_2O was used as solvent, the reaction procedure was as follow: (1) 10 mg isopropylamine were added to 10 mg AHA samples. [16] (2) After two hours of the addition of the isopropylamine, 5 mL of D_2O was added to the mixture. (3) The mixture was then sealed in a flask and left to react one to three days at 90-100° C. The final products were obtained by freeze drying the mixture overnight.

Synthesis of Copper(II), Iron(III)-Catechol Model Complexes

In order to better understand the behavior of AHA, catechol was chosen as a model compound of AHA because it is a major component of AHA. We made the metal-catechol model complexes at the same three conditions as that for metal-AHA complexes.

Fe^{3+} and Cu^{2+}-catechol complexes at condition I and II were made by mixing 0.965g catechol with 10ml of 2M $CuCl_2$ or $FeCl_3$ at 60-70° C or room temperature for 24-72 hrs. The ratio of catechol to Cu^{2+} or Fe^{3+} was 1mole to 2.28moles. The final products of Cu^{2+} and Fe^{3+}-catechol complexes were washed with a HCl water solution at pH=1, centrifuged and freeze dried for 24 hrs. The complexes were found to be black powders.

Fe^{3+} and Cu^{2+}- catechol complexes at condition III were made by mixing 0.55g catechol samples with 10 mL of 0.36 M $Cu(OAc)_2$ in a ratio of 1mole catechol to 0.72mole Cu^{2+} at pH =6. The reaction was run at room temperature for 72 hrs. The Fe^{3+}-catechol complex was made by mixing 0.33 g catechol samples with

150 mL of 0.002 M $Fe(OH)_3$ aqueous slurry (pH=7) at room temperature for 72 hrs. The ratio of AHA to Cu^{2+} or Fe^{3+} was 10 moles to 1 mole. Both were washed with deionized water, centrifuged, and freeze dried for 24 hrs, yielding a black powder as final product.

Table 3.3 showed the measured element amounts and proposed structures of Cu^{2+}-catechol model complexes at the above three conditions.

Table 3.3 Elemental Analysis Data and Proposed Structures of Cu^{2+} and Fe^{3+} -Catechol Model Compounds

element analysis	Cu^{2+}-catechol complexes at conditionI	Cu^{2+}-catechol complexes at condition II	Cu^{2+}-catechol omplexes at condition III
	Exp.	Exp.	Exp.
C%	55.87	48.30	44.46
H%	2.60	2.41	2.69
Cu%	3.51	13.96	21.92
Cl%	0.00	0.00	0.00
element analysis	Fe^{3+}-catechol complexes at condition I	Fe^{3+}-catechol complexes at condition II	Fe^{3+}-catechol omplexes at condition III
	Exp.	Exp.	Exp.
C%	45.82	56.44	45.81
H%	2.073	2.22	2.72
Fe%	6.907	4.45	16.40
Cl%	10.54	3.90	14.70
Proposed structure	Cu^{2+} and Fe^{3+} - polymeric quinone complexes	Cu^{2+} and Fe^{3+}- polymeric semiquinone complexes	Cu^{2+} and Fe^{3+}- semiquinone complexes

Discussion

AHA has the capacity to sorb a variety of inorganic species such as heavy metal cations and reducible metal cations Cr^{6+}, Fe^{3+}, and Cu^{2+}. To elucidate the metal cation-AHA interaction mechanisms we characterized and simulated the functional groups found in the AHA followed by a study of interaction mechanisms between these functional groups and the metal cations. A model for AHA molecular structure was proposed by Stevenson[8] (Figure 3.1) and they indicated that the functional structures of AHA are mainly catechol analogues and phthalic acid analogues. Between the two main functional groups of AHA, catechol and phthalic acid analogues, we believed that the catechol functional groups are more important for metal cation adsorption due to their strong chelation. Based on this we have chosen catechol as a relevant model compound for AHA. Cu^{2+} and Fe^{3+} are typically reducible metal cation contaminants in the subsurface system which can interact with AHA by reduction-chelation. Therefore, we set out to study the interaction mechanisms of Cu^{2+} and Fe^{3+}-AHA complexes and Cu^{2+} and Fe^{3+}- catechol model complexes. These studies may contribute to the better understanding of the actual metal ion adsorption and interaction processes of HA in groundwater system.

Functional group Structure Study

FTIR Spectroscopic Study

FTIR spectra of AHA and humate were taken to identify the characteristic peaks of AHA (Figure 3.2A and 3.2B). The humate was the AHA-sodium salt and AHA was produced by washing the humate by a HCl solution at pH=2. It was found that after acid washing, the bands at 1580 cm^{-1} and 1381cm^{-1}, asymmetric and symmetric COO^- stretch (Figure 3.2B),[17, 18] shifted to 1715 cm^{-1}. This band can be assigned to the carboxylic acid C=O stretch (Figure 3.2A).[17, 18] Therefore, the FTIR spectra clearly indicated the existence of COOH functional groups of AHA.

The FTIR spectrum of AHA also showed bands at 1615cm^{-1} (ring mode), 1180-1395 cm^{-1} (OH bending of aromatics and C-O stretch of aromatics and carboxylic acid), bands at 1395-1480 cm^{-1} (OH deformation of carboxylic acid and ring stretch), the moderate peak at 1033 cm^{-1} (poly-substituted benzene

rings), and a broad peak at 3000-3683 cm⁻¹ region (CH stretch, OH stretch of aromatics, and OH stretch of carboxylic acid analogues).[17, 18]
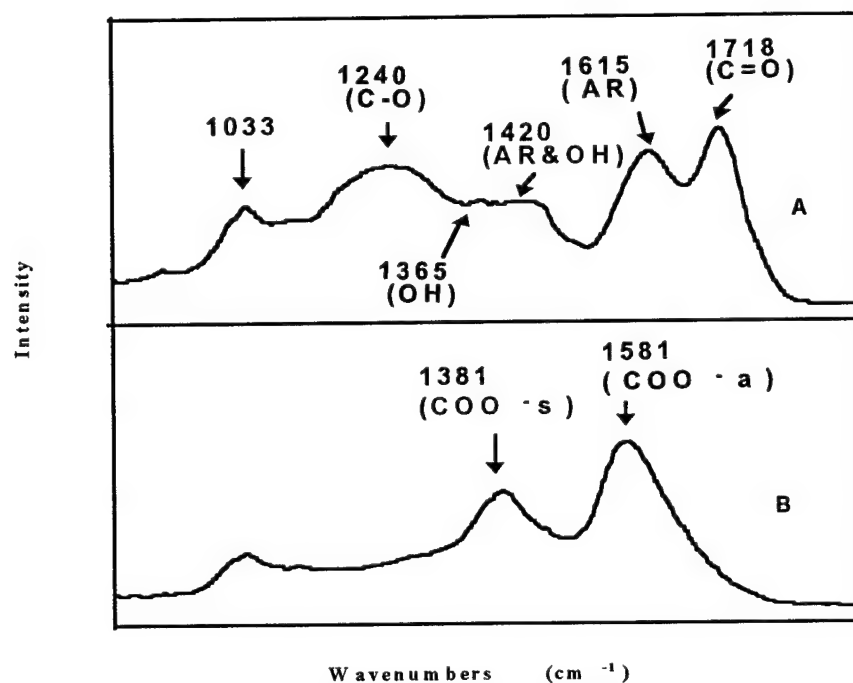

Figure 3.2 FTIR Spectra A. AHA. B. Na-Humate

Table 3.4 shows the FTIR peak assignments of the AHA. FTIR bands of AHA, including the aromatic OH and COOH as well as those suggesting poly-substituted aromatic structure are all consistent with the structure proposed by Stevenson.[8]

Table 3.4 Transmittance FTIR Band Assignments [17,18,19,20,21] of AHA and d-Isopropylammioum Humate

AHA (cm^{-1})	d-isopropylammioum humate(cm^{-1})	Assignments
3200-3617		OH and CH stretch of catechol
3000-3617		OH and CH stretch of aromatic carboxylic acid
	2737	OD stretch
	2537	OD stretch
	2111	OD stretch
2920	2920	CH stretch
2850	2850	CH stretch
1715		C=O stretch
1615		ring mode
	1578	COO⁻ asymmetric stretch
	1389	COO⁻ symmetric stretch
1395-1520		OH deformation of carboxylic acid & ring mode
	1466	ring mode
1115-1395		OH bending of catechol C-O stretch of aromatics & carboxylic acid
	1222, 1165	C-O stretch of catechol
1033	1033	poly-substituted benzene ring mode

Deuteration

If the hypothesis of catechol analogues in AHA is correct, we should observe the characteristic bands similar to those found in the pure catechol. We took the FTIR spectra of pure catechol and AHA (Figure 3.3A and 3.3B). Figure 3.3A has the following peaks which are of interest: 1365 cm^{-1} (OH bending of catechol), 1187-1280 cm^{-1} region (C-O stretch),and 1470-1530cm^{-1} (ring mode).[17, 18, 19, 20, 21] However, Figure 3.3B is difficult to characterize due to the broad absorptions of AHA which are caused by the multiplicity of the similar sites. This makes it difficult to clearly see the characteristic OH bending, C-O stretch, and ring modes of catechol analogues. To overcome this, the sample was isotopic substituted to cause band shifts for the OH groups of catechol and carboxylic acids. At the same time, the sample was reacted with isopropylamine to cause carboxylic acid C-O band shift by carboxylate formation. Therefore, the characteristic bands we expect to see might be revealed. Figure 3.4 illustrates the deuteration of AHA and the model compounds catechol and carboxylic acid. Figure 3.5 shows the formation of isopropylamminoum humate.
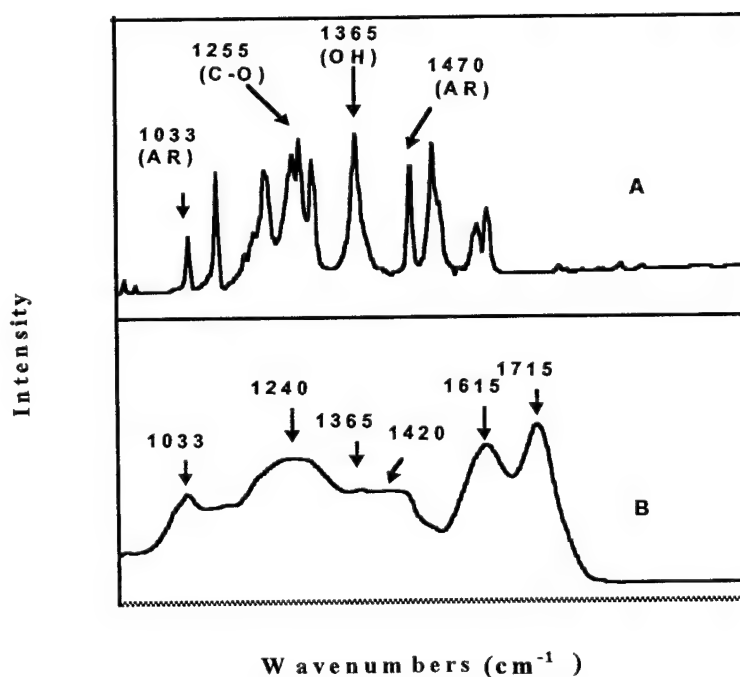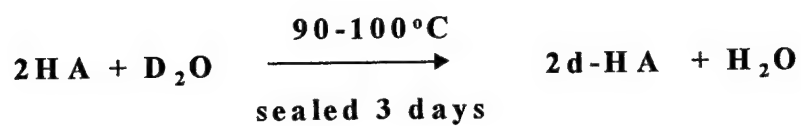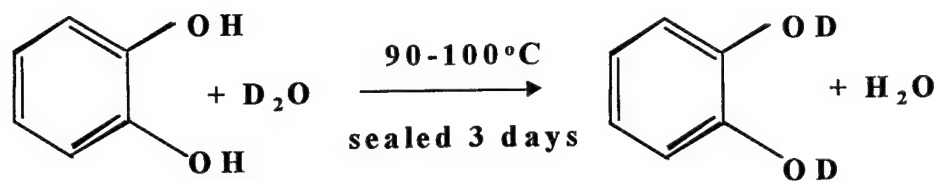

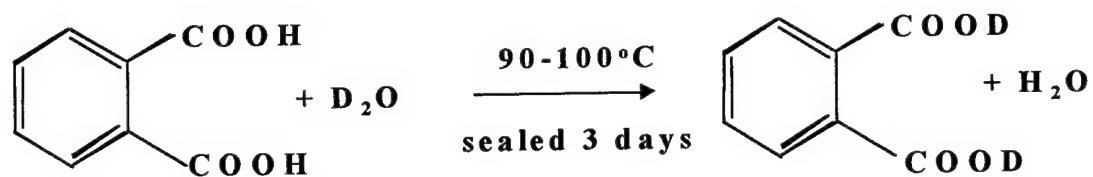**Figure 3.3. FTIR spectra (A) pure catechol (B) AHA**

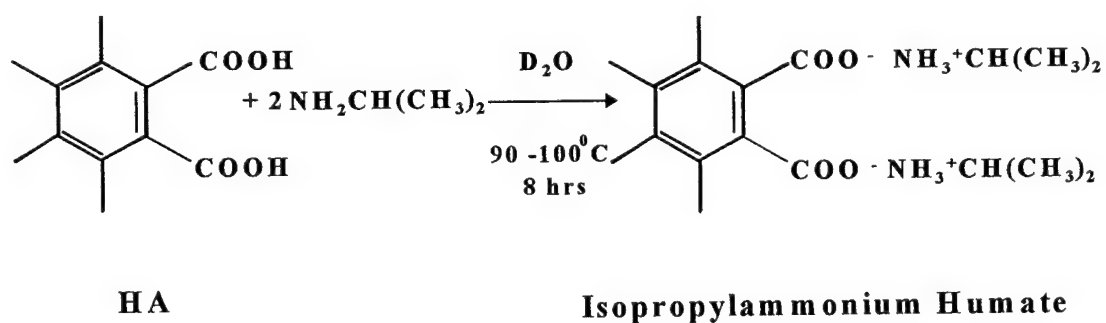**Figure 3.4 Deuteration of phthalic acid, catechol, and AHA**

Figure 3.5 Formation of isopropylammonium humate

37

FTIR spectra of AHA, d-isopropylammonium humate, and d-catechol are shown in Figure 3.6A, 3.6B, and 3.6C, respectively. In Figure 3.6B, it is noticed that, after deuteration and a targeted reaction, bands which used to be in the 3000-3683 cm^{-1} region (OH stretch of carboxylic acid and catechol analogues) were shifted to the 2100-2700 cm^{-1} region (OD stretch of carboxylic acid and catechol analogues).[18] The broad band which used to be in the 1520-1395 cm^{-1} region (OH deformation of carboxylic acid and ring mode) appeared at 1466 cm^{-1} (ring mode of AHA).[17, 19, 20, 21] The bands at a 1115-1395 cm^{-1} region are catechol C-O stretches, carboxylic acid C-O stretch, and OH bending. After isopropylamminoum carboxylate formation, the C-O stretch of carboxylic acid is shifted, and the peaks revealed at 1222 cm^{-1} and 1165 cm^{-1} are C-O stretches of catechol. [17, 19, 20, 21] The peak attributed to the poly-substituted benzene rings remained at 1033 cm^{-1} regions without any change after deuteration.

A.   H A
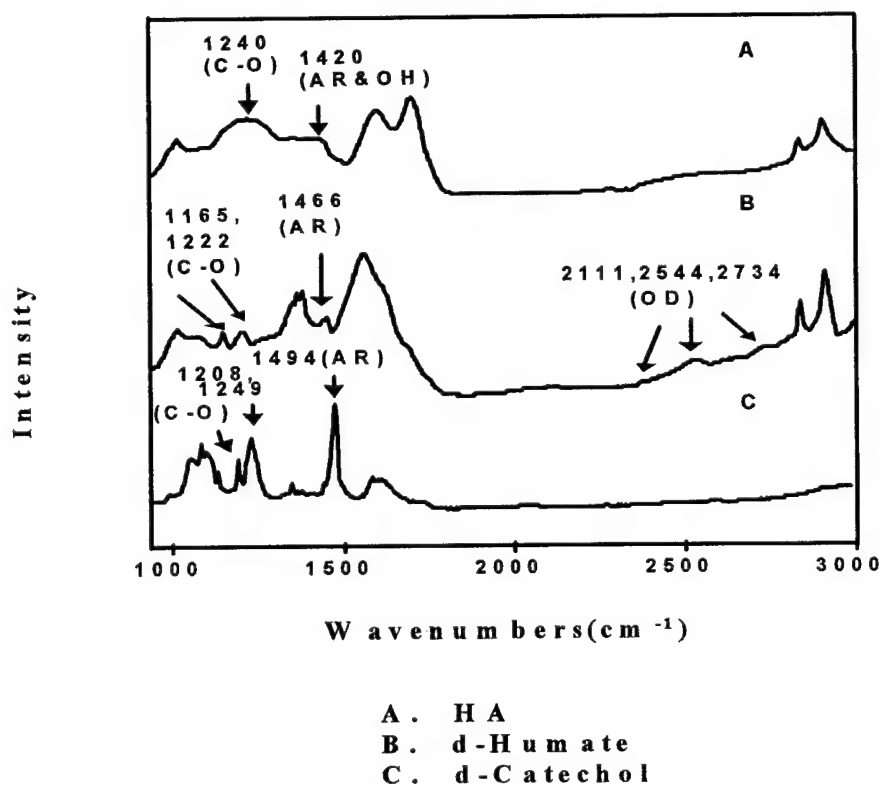B.   d -H um ate
C.   d -C atech o l

Figure 3.6 FTIR spectra

A comparison of the C-O stretch and ring mode bands in d- isopropylammonium humate with those in d- pure catechol reveals similarity in these spectra. The possible C-O stretch of catechol analogues in d-isopropylammonium humate showed up as two bands (1222 cm^{-1} and 1165 cm^{-1}). The C-O stretch of d-catechol also showed up as two bands (1249 cm^{-1} and 1208 cm^{-1}). Furthermore, the possible ring modes for both d-catechol and d- isopropylammonium humate appeared at 1493 cm^{-1} and 1466 cm^{-1}, respectively. However, it is seen that the C-O stretch and ring modes for both d-catechol and d- isopropylammonium humate didn't show at exactly the same frequencies. We believe that the behaviors of both pure catechol and AHA could not be exactly the same, because AHA are multiple-substituted macromolecules and catechol is not. Therefore, our studies lend credence to our hypothesis that catechol analogues might be important components in AHA.

Oxidation Study

Catechol can be oxidized by reducible metal cations, such as Cu^{2+} and Fe^{3+} to form quinone (Figure 3.7).[9] If catechol-like components are functional groups of AHA, the AHA should also undergo a similar oxidation-chelation reaction. Therefore, in another attempt to determine if catechol analogous structures exist in AHA and how AHA interacts with metals, we reacted metal cations with both AHA and catechol to examine if the analogous oxidation occurred. From the previously proposed model structure of AHA (Figure 3.1), the possible functional groups of AHA, including carboxylic acid analogues are not likely to be further oxidized with the exception of the catechol-like groups.
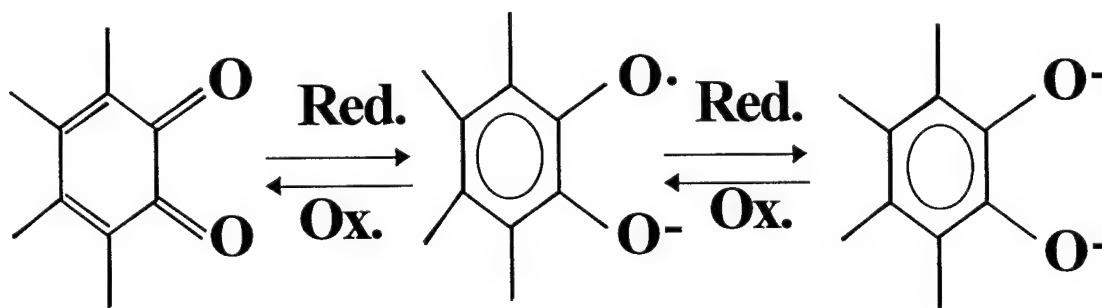

Figure 3.7 Oxidation reaction of AHA

Jones et al.[22] found that the C=O stretch frequency of ortho-diketones is at 1726 cm, and the conjugation effect of a C=C double bond will reduce the C=O stretch slightly and should show up at 1700-1720 cm^{-1} region. However, the carboxylic acid structure of AHA also could show the C=O stretch at 1700cm^{-1} region.[17, 18] The deuteration of the pure carboxylic acid showed no shift for this C=O stretch peak (Figure 3.8). Therefore, isopropylamine was also used as a reagent to react with Fe^{3+} oxidized AHA to form isopropylammonium humate. After the reaction, the C=O stretch of carboxylic acid showed up as symmetric and asymmetric COO$^-$ forms at 1578 cm^{-1} and 1389 cm^{-1} due to the transformation of carboxylic acid to carboxylate. The reaction is shown in Figure 3.5.
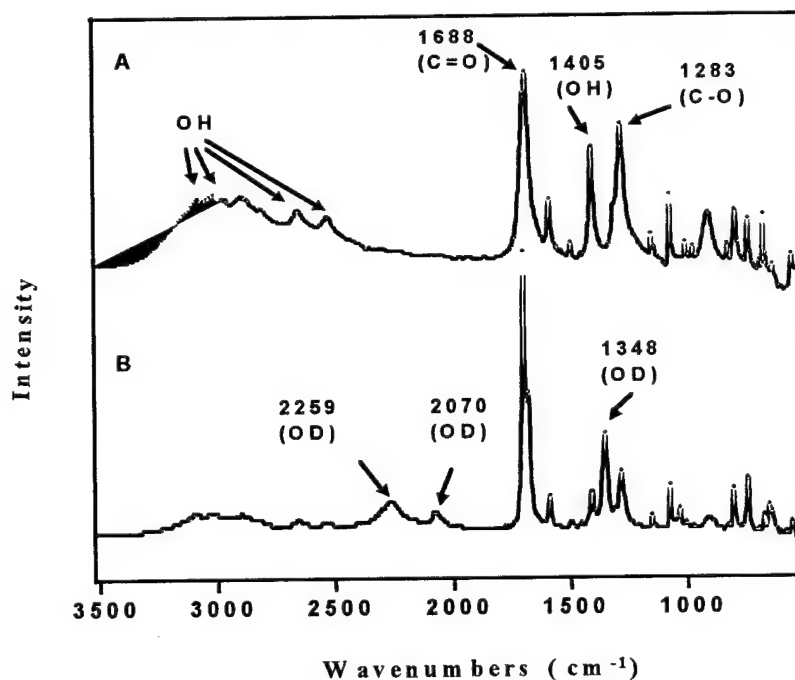
Figure 3.8 FTIR spectra
(A) carboxylic acid
(B) d-carboxylic acid

Figures 3.9 A and 3.9 B are FTIR spectra of the Fe^{3+} oxidized isopropylammonium humate and Fe^{3+} oxidized catecholate, respectively. The spectra show many similarities. Both exhibit peaks at 1718 cm^{-1}. We believe that the band at 1718 cm^{-1} are the C=O stretch of ortho-quinone in both Fe^{3+} oxidized AHA and catechol.
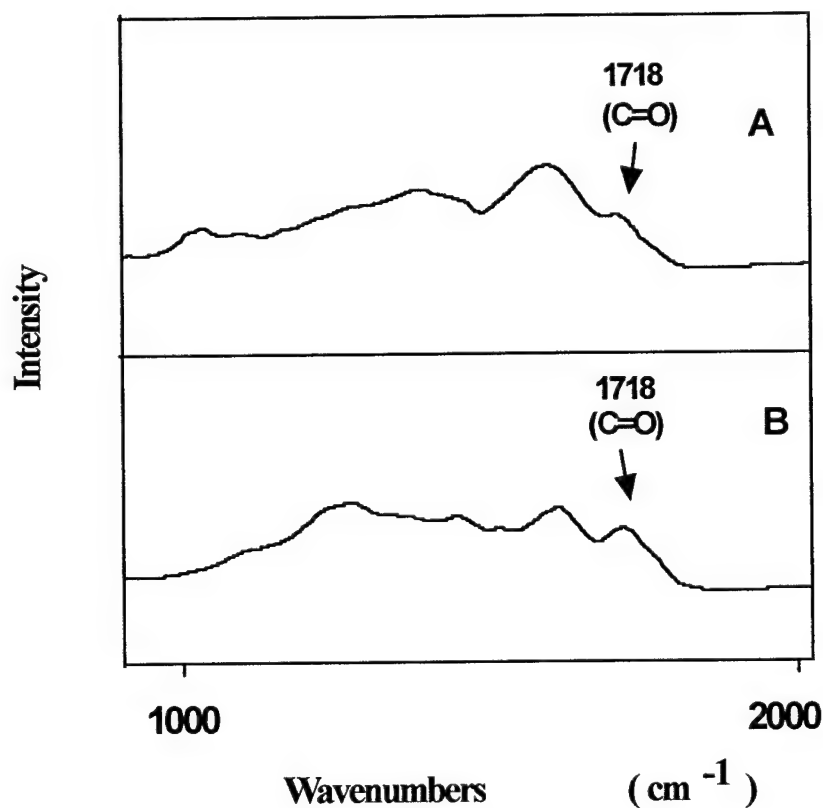
A. d-Fe^{3+} oxidized isopropylammonium humate
B. d-Fe^{3+} oxidized catecholate

Figure 3.9 FTIR spectra

41

Figure 3.10 A and B are the FTIR spectra of Fe^{3+} oxidized isopropylammonium humate and isopropylammonium humate, respectively. By comparing them, we can clearly see that AHA can be oxidized by Fe^{3+} to form quinone which showed its C=O stretch peak at $1718 cm^{-1}$. When we subtracted the FTIR spectrum of isopropylammonium humate (Figure 3.10 B) from that of Fe^{3+} oxidized isopropylammonium humate (Figure 3.10A), obtained the FTIR spectrum in Figure 3.10C.
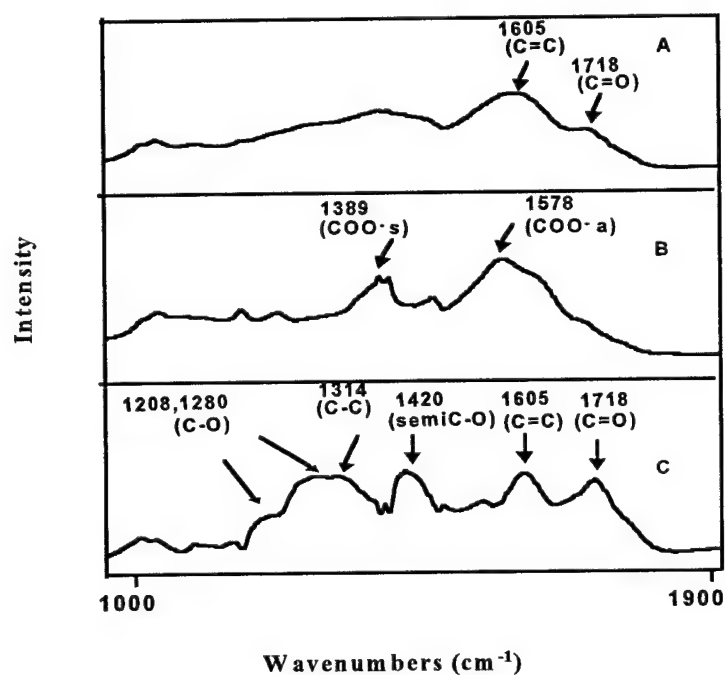
A. d- Fe^{3+}oxidized isopropylammonium humate
B. d-Isopropylammonium humate
C. subtraction of (A) minus (B)

Figure 3.10 FTIR spectra

Figure 3.10C clearly shows the formation of quinone and catecholate (or semiquinone) of Fe^{3+} oxidized AHA, evidenced by the FTIR peaks at $1718 cm^{-1}$ (quinone C=O stretch), $1605 cm^{-1}$ (C=C stretch of C=C-C=O

structure),1400-1480cm^{-1} region (peak 1420cm^{-1}) (semiquinone C-O stretch [23]), 1314cm^{-1} (C-C stretch of quinone), and 1208-1280cm^{-1} region (C-O stretch of catecholate). The subtracted peak assignments are listed in Table 3.5.

Therefore, catechol and carboxylic acid analogues are present as primary structural components of AHA. These data are consistent with the structure for AHA proposed by Stevenson. [8]

Table 3.5 Transmittance FTIR Band Assignments [17, 18, 19, 20, 21] of Subtraction of d-Fe^{3+} Oxidized Isopropylammonium Humate minus d-Isopropylammonium Humate

d-Fe^{3+} oxidized isopropylammonium humate minus d-isopropylammonium humate (cm^{-1})	Assignments
1718	free quinone C=O stretch
1605	C=C stretch of C=C-C=O
1420 (1400-1480 region)	semiquinone C-O stretch
1314	C-C stretch of quinone
1208 , 1280	C-O stretch of catecholate

Coordination Ability of AHA with Metal Cations

To determine the metal coordination ability of AHA we measured the concentrations of coordinated metal cations in the Fe^{3+} and Cu^{2+}-AHA complexes. It was found that the percentage of coordinated metal cations (Table 3.2) was influenced by the characteristic configuration and functional groups of AHA which can be affected by solution pH and reaction temperature. The experiments showed that the concentrations of Fe^{3+} and Cu^{2+} coordinated at condition III are much higher than that at condition I and II.

Considering the configuration and coordination behavior of AHA, we believed that the AHA is analogous to a polyelectrolyte. [12, 13, 14, 15] Due to the hydrolysis at condition I and II, the majority of the main

functional groups exist as COOH and OH forms which were unfavorable to the metal ion coordination. Solvating cations can easily minimize the repulsion due to charge on adjacent carboxylate and hydroxylate groups. This leads to a coiled configuration of the AHA[7, 12, 15] with few active sites available for coordination with Cu^{2+} and Fe^{3+} metal cations.[24, 25] However, at condition III, due to the hydrolysis, the functional groups exist in the COO^- and O^- forms, and the AHA may adopt a more open configuration in solution as a result of charge repulsion between ionized functional groups.[26, 27, 28] This extended configuration has been reported to create more active sites for metal coordination (Figure 3.11).[28]
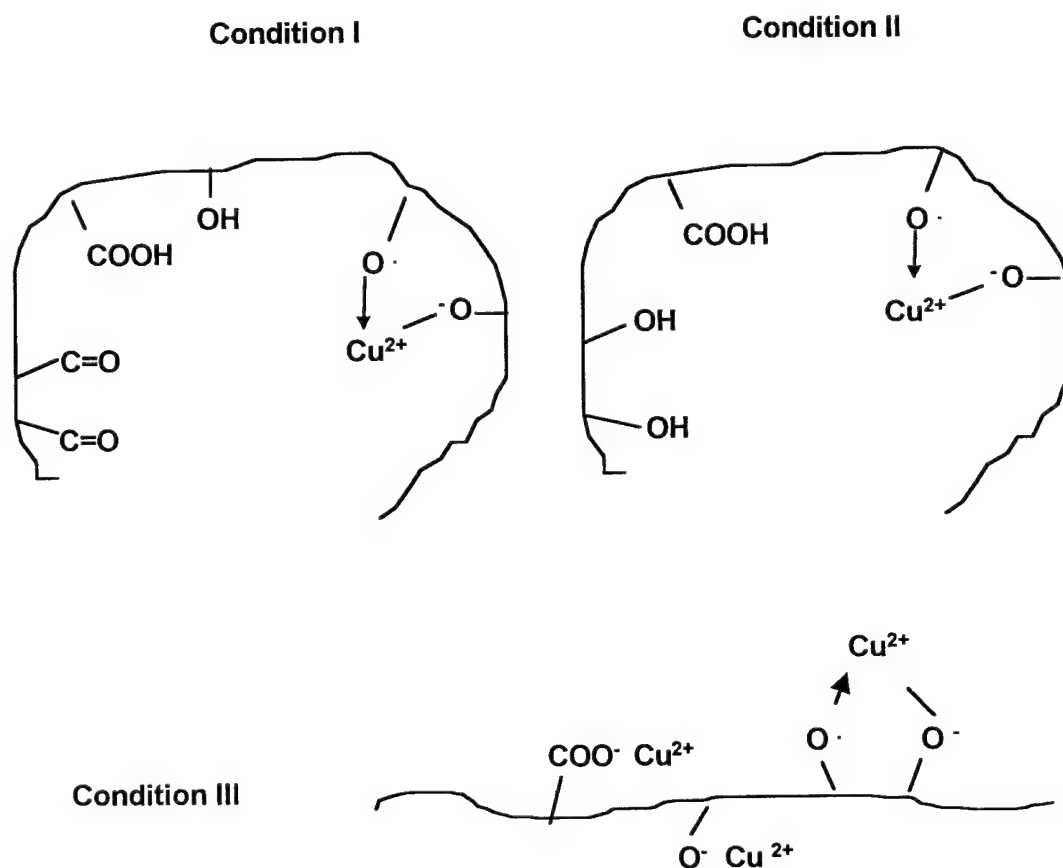

Figure 3.11 The configuration of AHA at different pH conditions

44

The effect of solution pH on the AHA's metal coordination ability is also evidenced by FTIR spectra. It was found that FTIR spectra of Cu^{2+}-AHA complexes were similar to Fe^{3+}-AHA complexes at the same conditions. Figure 3.10A is the FTIR spectra of Fe^{3+} oxidized isopropylammonium humate at condition I, Figure 3.12A and B are the FTIR spectra of Fe^{3+} oxidized AHA and Fe^{3+} oxidized isopropylammonium humate at condition II, Figure 3.12C and D are the FTIR spectra of Cu^{2+} oxidized AHA and Cu^{2+} oxidized isopropylammonium humate complexes at condition III. It was found that the quinone structure (1718 cm^{-1} in Figure 3.10A) formed at condition I existed as free quinone form without further metal coordination because a coordinated C=O stretch should be shifted 60 cm^{-1} to lower wavenumber than that of the free C=O [23] and no peak is seen in this region (Figure 3.10A). At condition II, the peak at 1718 cm^{-1} (Figure 3.12A) is assigned to the uncoordinated COOH functional groups because this peak shifted after deuteration and the targeted reaction. Furthermore, we can see a broad weak OH peak at 1365 cm^{-1} which indicated the unreacted OH groups (Figure 3.12 A). Comparison of the three conditions shows that the solution pH and temperature can affect the functional group structures and configuration of AHA and thus affect its metal coordination ability.
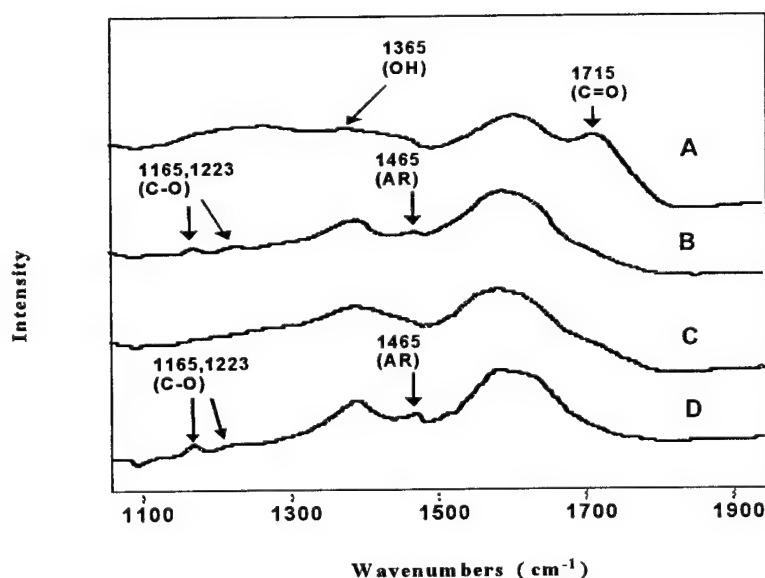

Figure 3.12 FTIR spectra

A. Fe^{3+}-AHA complexes.
B. Fe^{3+}- isopropylammonium humate complexes
C. Cu^{2+}-AHA complexes.
D. Cu^{2+}-isopropylammonium humate complexes

45

Oxidization Mechanism of AHA

From our research, we found that catechol functional group of AHA can be oxidized to form semiquinone and quinone structures. In order to investigate the oxidization-reduction mechanism we examined the $E°$ and E values of the related reactions (Table 3.6 [29, 30, 31,32]). From Table 3.6 we found that the oxidation of catechol to quinone is a two- step reaction with different E values. The E values of $HQ^. + H^+ + e \rightarrow H_2Q$ at pH=1 condition is smaller than that of Cu^{2+} and Fe^{3+} which indicates that the electron transfer from catechol to Cu^{2+} and Fe^{3+} is preferred. However, the E value of $Q + H^+ + e \rightarrow HQ^.$ at pH=1 condition is larger than that of Cu^{2+} / Cu^+ which means that the oxidization of semiquinone to quinone is not performed directly by the reduction of Cu^{2+}. We proposed that the reduction of O_2 is involved in these two step oxidation reactions and the Cu^{2+} and Fe^{3+} are acting as catalysts. [9, 31, 32] Pierpont et al. [9] indicated that the charge transfer contributes significantly to the features of iron-catecholate coordination, and it is responsible for the unique stability of Fe^{3+}(Cat) chelates and the activation of catecholate ligands toward O_2 oxidation.

Table 3.6 E^0 and E Values of Compounds and the Related Redox Reactions [29, 30, 31, 32]

Redox Reactions	E^0 and E value
$O_2 + 4 H^+ + 4 e^- \rightarrow 2H_2O$	1.17 (pH=1), 0.87(pH=6)
$O_2 + 2 H^+ + 2 e^- \rightarrow H_2O_2$	0.62 (pH=1), 0.32(pH=6)
$H_2O_2 + 2 H^+ + 2 e^- \rightarrow 2H_2O$	1.71 (pH=1)
$Fe^{3+} + e^- \rightarrow Fe^{2+}$	0.70 (pH=1)
$Cu^{2+} + e^- \rightarrow Cu^+$	0.16
$HQ^. + H^+ + e^- \rightarrow H_2Q$ (Hydroquinone)	-0.249(pH=1) 0.341 (pH=6) [31,32]
$Quinone + H^+ + e^- \rightarrow HQ^.$	0.454 (pH=1) 0.158 (pH=6) [31, 32]

Molecule Structure Study of Cu^{2+}, Fe^{3+} -Catechol Model Complexes

AHA is a complicated macromolecule. Although the study of Cu^{2+} and Fe^{3+}-AHA complexes gave us basic information about the metal interaction of AHA, the investigation of metal-catechol model complexes can give us a better understanding about the metal-AHA coordination mechanisms. In this study we examined the characteristics of metal coordination of catechol model compounds since catechol analogues represent many structures of AHA. The catechol-metal model studies were conducted at the same three conditions as that used with the AHA. However, catechol chemistry is complicated. Researchers have found that catechol can be oxidized by Cu^{2+} and Fe^{3+} to form four kinds of compounds: [33, 34, 35, 36] (1) quinone and semiquinone, which are formed by the oxidation of catechol; (2) metal cation-catecholate or semiquinone complexes; (3) muconic acid, formed by free quinone ring opening without the existence of any metal cations; and (4) polymers formed by polymerization of semiquinone.

Although previous work indicated that catechol can be oxidized by Cu^{2+} and Fe^{3+} to form polymers, [10, 11, 34, 35, 36] those studies did not provide structures of the polymers. We investigated and modeled the structures of metal-polymeric catechol complexes based on the FTIR spectroscopic study, ESR spectra, and elemental analysis. The FTIR spectra of these metal-catechol model complexes at condition I, II and III are shown in the Figure 3.13, 3.14, and 3.15, respectively.

The FTIR spectra of metal-catechol complexes contain macromolecular characteristics evidenced by the broad FTIR peaks (Figure 3.9A and 3.9B). The element analysis results (Table 3.3) also showed that the hydrogen of the catechol ring was substituted, which could be caused by polymerization. Based on these results we believed that the oxidation of catechol was followed by polymerization.
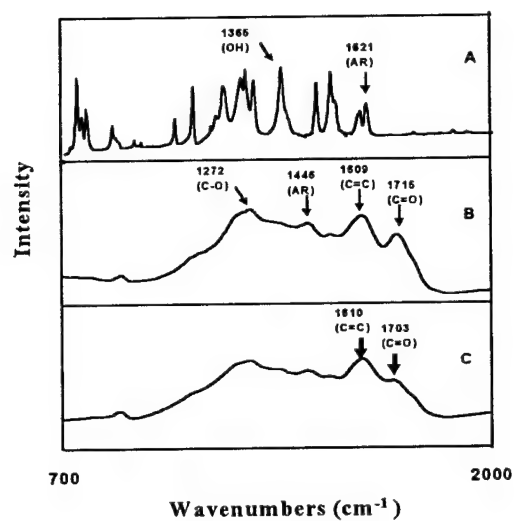
A. Pure catechol
B. Fe³⁺-catechol complexes
C. Cu²⁺-catechol complexes

Figure 3.13 FTIR spectra of

metal-catechol complexes
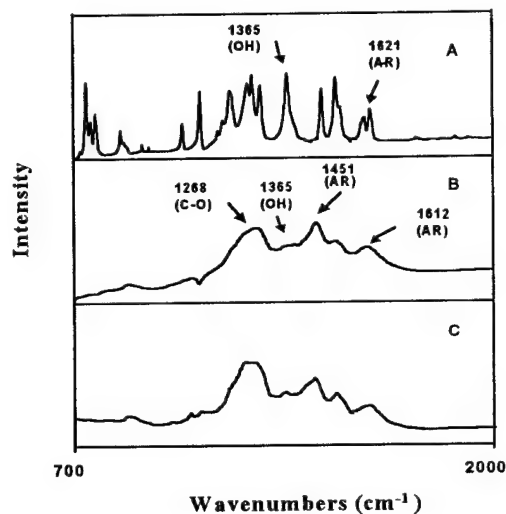
at condition I

A. Pure catechol
B. Fe³⁺-catechol complexes
C. Cu²⁺-catechol complexes

Figure 3.14 FTIR spectra of
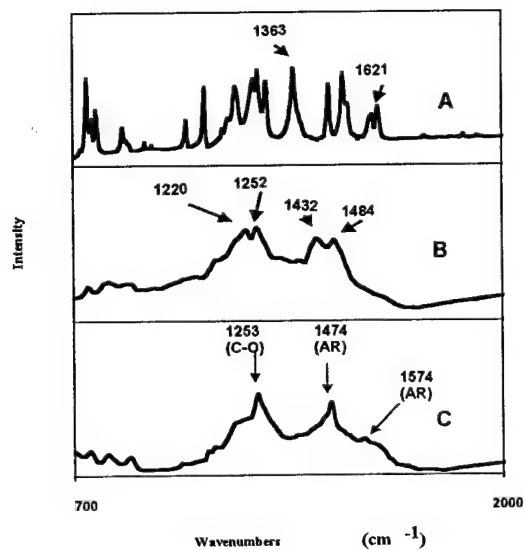
metal-catechol complexes

at condition II

A. Pure catechol
B. Fe³⁺-catechol complexes
C. Cu²⁺-catechol complexes

Figure 3.15 FTIR spectra of metal-catechol complexes at condition III

48

Table 3.7 is the peak assignments of iron (III)-catechol complexes at all three conditions.

Table 3.7 Transmittance FTIR Band Assignments[17, 18, 19, 20, 21] of Fe^{3+} - Catechol Model Compounds at Conditions I, II, and III

Fe^{3+}-catechol complexes at conditions I (cm^{-1})	Fe^{3+}-catechol complexes at conditions II (cm^{-1})	Fe^{3+}-catechol complexes at conditions III (cm^{-1})	Assignments
1715			free quinone C=O stretch
1609			C=C stretch of C=C-C=O
1446			ring mode or semiquinone C-O stretch
1272			C-O stretch of catecholate
	1612		C=C stretch of C=C-C=O
	1513		ring mode
	1451		ring mode or semiquinone CO
	1365		OH bending
	1268		C-O stretch
		1432-1484	ring mode or semiquinone C-O stretch
		1220-1252	C-O stretch of catecholate

Formation of Fe^{3+} and Cu^{2+} - Polymeric Quinone and Semiquinone Complexes at Condition I and II

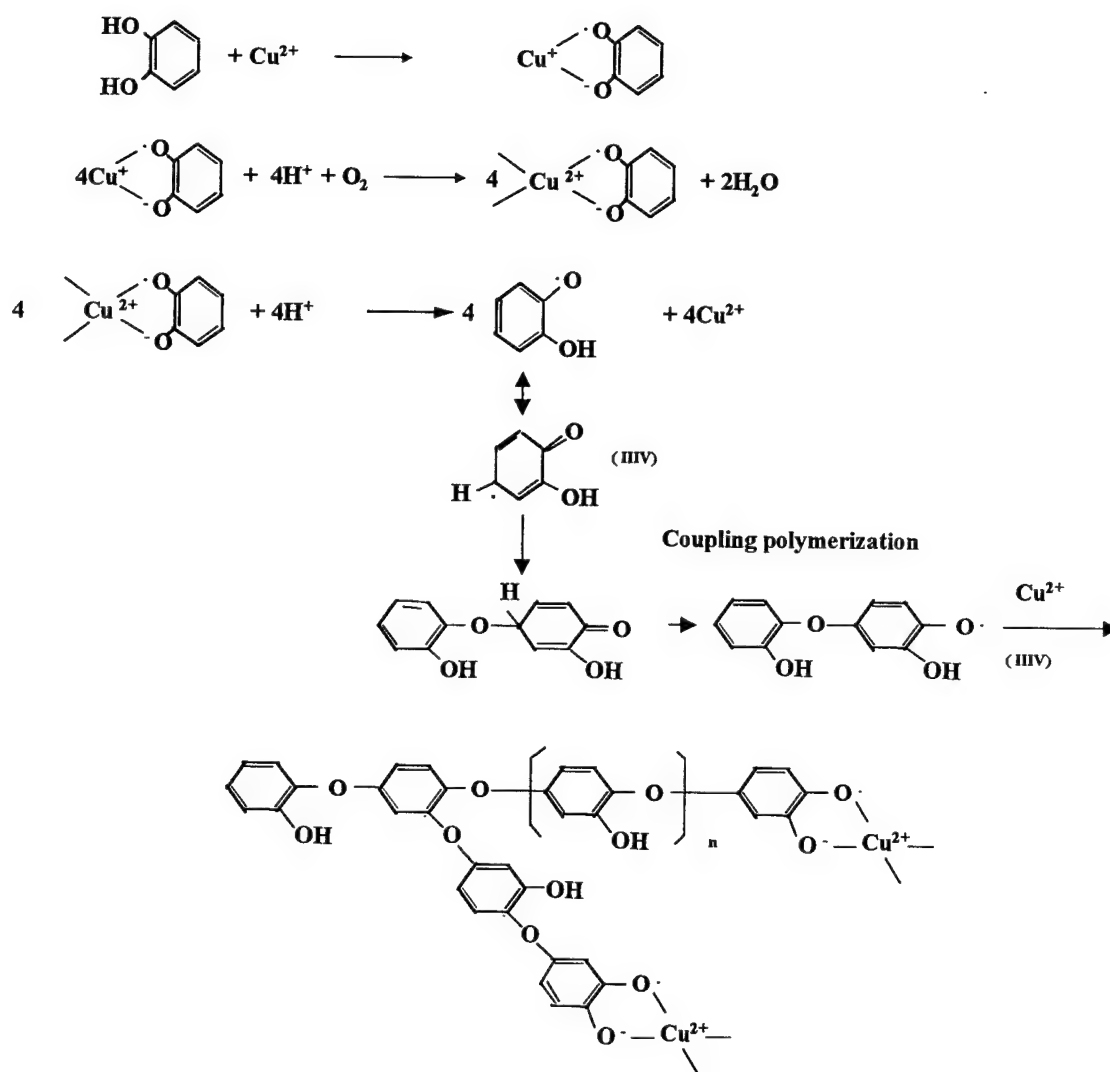The FTIR spectra of pure catechol, Cu^{2+} and Fe^{3+}-catechol complexes at conditions I and II are shown in Figure 3.13 and 3.14 A, B, C, respectively. The FTIR spectra of metal-catechol complexes contain a broad peak at 1200-1700cm^{-1} region which is similar to that of AHA. The elemental analysis results of Cu^{2+} and Fe^{3+}-catechol complexes at conditions I and II showed the H/C ratio of less than 0.0555 which are lower than that of the catecholate structure (4H / 6C=0.0555). Therefore, results from both element analysis and FTIR spectra indicate polymerization of catechol. Due to the quinone C=O peak in the FTIR spectrum of polymeric catechol-metal complexes at condition I, we believed that these complexes are formed by oxidative coupling polymerization of catechol followed by dimerizationor further oxidation.[37] Similarly, at condition II, because no quinone C=O peak showed up at the FTIR spectrum, we believed that it is only oxidative coupling polymerization of catechol.[37] The oxidative coupling polymerization mechanisms and the model molecule structures of Cu^{2+}- polymeric catechol complexes at conditions I and II are proposed in Figure 3.16 and 3.17, respectively.[37] We proposed that oxidation of catechol to semiquinone is accomplished under oxygen through catalytic metal-catecholate complexes at acidic condition, semiquinone is polymerized by coupling polymerization to form polymeric semiquinone, and polymeric semiquinone undergoes dimerization or further oxidation to form polymeric quinones.[9,37] This proposal is supported by the work done by Odian.[37] They indicated that the oxidative coupling polymerization of many 2,6-disubstituted phenols to form aromatic polyethers is performed by bubbling oxygen through a solution of the phenol in an organic solvent containing a catalytic complex of a cuprous salt and a tertiaryamine.
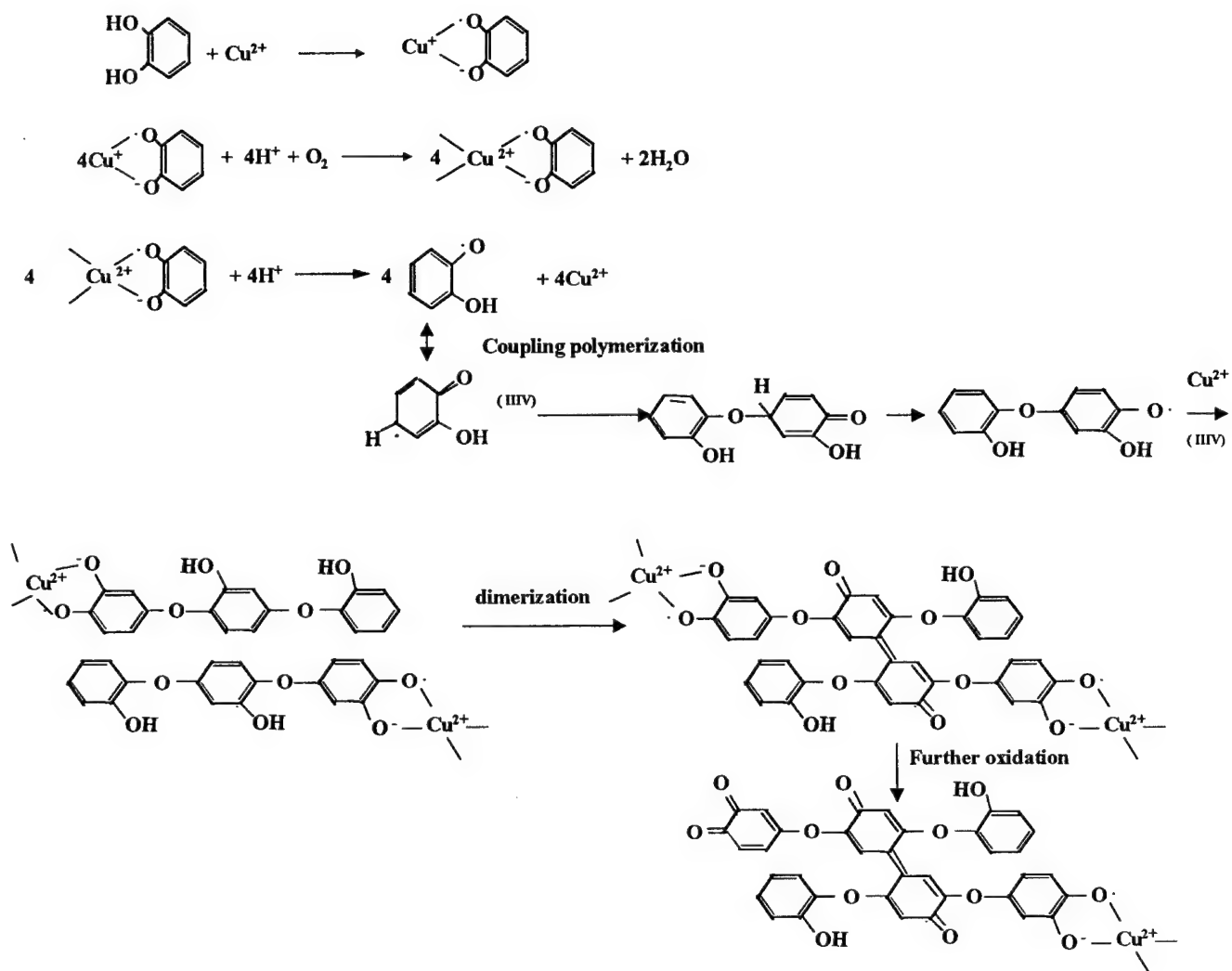
Condition I

Figure 3.16 Reaction mechanism of Cu^{2+}-catechol complexes at condition I

condition II

Figure 3.17 Reaction mechanism of Cu^{2+}-catechol complexes at condition II

When the reaction was performed at condition III we found that the H/C ratio is larger than 0.0555 which is larger than that of the catecholate structure (4H/6C=0.0555). This indicated that the complexes may not undergo polymerization, instead, Cu^{2+} and Fe^{3+}- catecholate or semiquinone complexes are formed. The FTIR spectra of pure catechol, neutral Cu^{2+} and Fe^{3+}-catechol complexes are shown in Figure 3.15A, B, and C, respectively. The bands at the $1450cm^{-1}$ region are catecholate ring modes or the C-O stretch of semiquinone and the peaks at $1268cm^{-1}$ are catecholate C-O stretches. [19, 20, 21, 22] We show their proposed structures and reaction mechanisms in Figure 3.18.
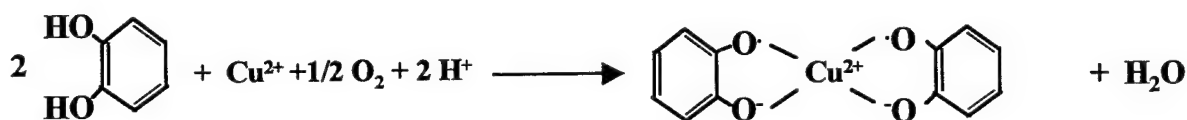
Figure 3.18 Reaction mechanism of Cu^{2+}-catechol complexes at condition III

Although we have modeled these complex structures, each of the complex structures proposed above may be considered only as one of the many possible structures of the catechol-Cu^{2+} and Fe^{3+} complexes. It is difficult to clearly identify the catechol-metal ion complex structures due to the complexity of the reactions. However, the model structures proposed here basically fit our FTIR spectra, element analysis results, ESR spectra results, and they can be considered as representative of the possible structures of the complicated catechol-Cu^{2+} and Fe^{3+} complexes.

Interaction Mechanism

Pierpont and Large [9] proposed that a strong catechol→Cu^{2+} and Fe^{3+} metal cation charge transfer (LMCT) would result in semiquinone characteristics for the coordinated catecholate ligand. To further investigate the interaction mechanism between metal cations and catechol we acquired ESR spectra for Cu^{2+}-catechol complexes (Figure 3.19A), and Fe^{3+}-catechol complexes (Figure 3.19B) under condition II. The g-values of these compounds are listed at Table 3.8. The ESR spectra of Cu^{2+}-catechol complexes contained characteristics of Cu^{2+}-semiquinone radicals [38] evidenced by their g-values at 2.0330 et al. Similarly, the ESR spectra of Fe^{3+}-catechol complexes showed g-values at 1.9988 and 4.2917 which indicated the formation of Fe^{3+}-semiquinone complexes.[38]

When we wash the Cu^{2+} and Fe^{3+}-catechol complexes with 35% HCl solution to remove the metal ions the ESR spectra clearly showed the free semiquinone radicals with g- factors at 2.0135 and 2.0000 (Figure 3.20). Therefore, it further proved that the complexes are Cu^{2+} and Fe^{3+}-semiquionone complexes.

We proposed that the interaction between semiquinone and Fe^{3+} and Cu^{2+} ions are the relatively weak intramolecular antiferromagnetic interaction.[39] The single unpaired electron of a o-semiquinone is located in a π-type molecular orbital as has been found in various molecular orbital calculation.[40] The unpaired electron of the o-semiquinone ligand is not directly involved in the bonding of the o-semiquinone ligand to the high-spin Fe^{3+} and Cu^{2+} ions. A lone pair of electrons on each oxygen atom of the o-semiquinone is used in the bonding to the metal.[39]

Table 3.8   g -Value of Fe^{3+} - Catechol Complexes and
Cu^{2+}- Catechol Complexes

Samples	Semiquinone g -Value	Metal Ion g-Value
Free semiquinone	2.0038-2.0048 [29]	
Fe^{3+}-catechol complexes	1.9988± 0.0008	4.2917±0.0008
Cu^{2+}-catechol complexes	2.0330± 0.0008	2.5798, 2.4354, 2.3145, 2.1829 ±0.0008
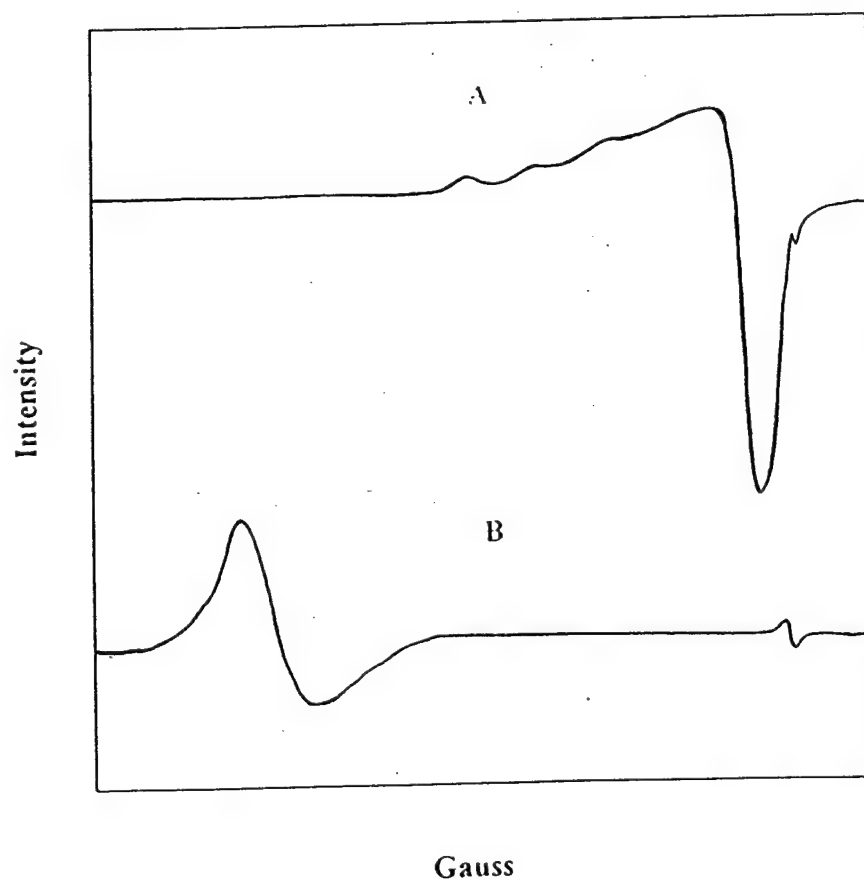
Figure 3.19 ESR spectra
(A) Cu^{2+}-catechol complexes
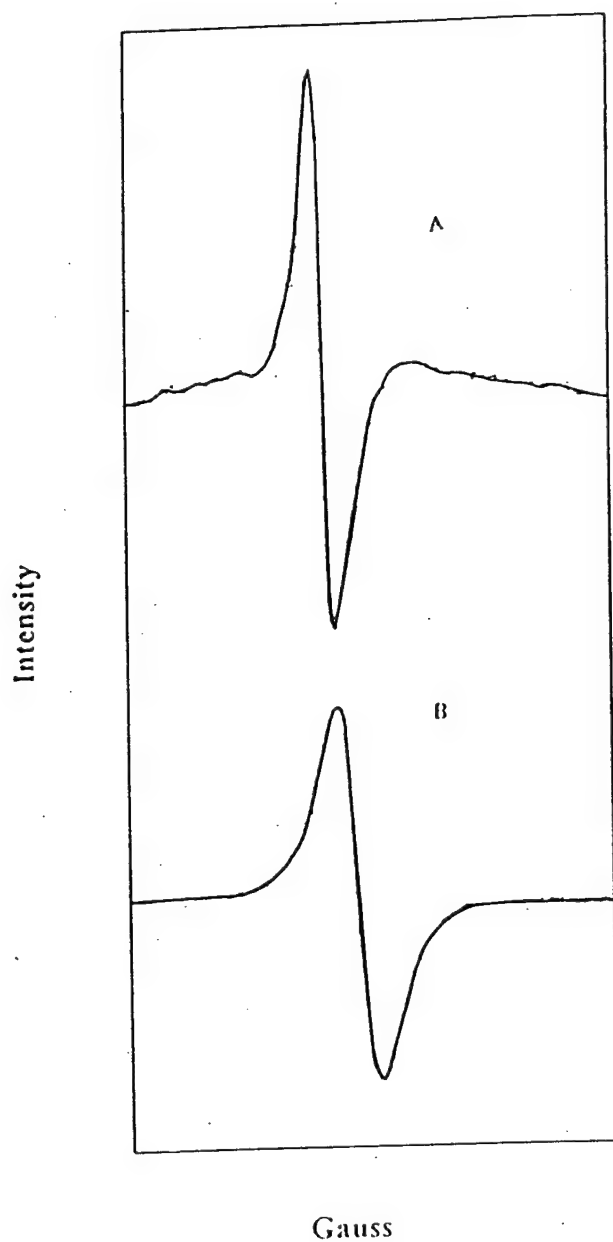**(B) Fe^{3+} - catechol complexes**

55

Intensity

Gauss

Figure 3.20 ESR spectra

(A) Cu²⁺-catechol complexes after 35% HCl washing

(B) Fe³⁺-catechol complexes after 35% HCl washing

56

Comparison of Coordination Behaviors of AHA and Catechol Model Compounds

AHA and model catechol compounds have similar metal coordination behaviors with respect to their coordination site selectivity, complex formation mechanisms, and coordination ability. At conditions I and II, both FTIR spectra of polymeric catechol and AHA showedsimilar macromolecular characteristics. Catechol can be oxidized to form semiquinone followed by polymerization, which is reminiscent of what is seen in AHA. The quinone structures for both catechol model compound and AHA formed at condition I existed as free quinone forms without further coordination, evidenced by the free quinone C=O peaks at $1718cm^{-1}$ (Figure 3.10A and 3.10B). At condition II, FTIR spectra of AHA and catechol model compound all showed the unreacted OH groups (Figure 3.14B,C and 3.12A). This indicated that the site selectivities of metal coordination for both AHA and catechol model compound are same.

The metal coordination abilities of both macromolecules are affected by the functional groups and the solution pH. At conditions I and II, the coordinating metal concentrations are small (Table 3.2) because portions of catechol analogues in AHA and catechol model compound are oxidized to form the quinone structure without metal coordination. Furthermore, the OH and COOH structures are unfavorable to coordinate metal cations at this strong acidic condition. Therefore, it is understandable that the coordinated metal concentrations of both catechol polymerization products and AHA are small.

Catechol model compounds and AHA show highest coordination ability at condition III, evidenced by the largest coordination metal concentrations in these complexes (Table 3.2). No peaks of unreacted OH functional groups are present in catechol and AHA (Figure 3.15B,C, and 3.12C). At condition III, the OH functional groups of AHA and model catechol sequestered the metal coordination more completely.

Conclusion

Three different methods -- deuteration, targeted chemical reaction, and oxidization followed by FTIR spectra analysis have shown that the AHA molecules mainly consist of two functional structures -- the carboxylic acid structure and catechol structure.

Carboxylic acid structures of AHA are unfavorable for coordination with metal cations to form complexes at acidic conditions. It is the catechol analogues of AHA which dominate the metal coordination reactions at acidic conditions. It has been also found that the quinone structures formed at condition I by the oxidization of AHA prefer to exist as free quinone form without further metal coordination. Therefore, site selectivity for the metal coordination is affected by functional group characteristics and solution pH. The coordinated metal concentrations of AHA are larger at condition III than that at condition I and II.

An ESR study indicated that the semiquinone-Cu^{2+} and Fe^{3+} complexes formed by the oxidation-reduction and chelation between metal cations and catechol. We proposed that O_2 is involved in the oxidization of AHA and catechol and that metal ions act as catalysts and chelates. The interactions between semiquinone and Fe^{3+} and Cu^{2+} ions are the relatively weak intramolecular antiferromagnetic interaction. The unpaired electron of the o-semiquinone ligand is not directly involved in the bonding of the o-semiquinone ligand to the high-spin Fe^{3+} and Cu^{2+} ions. A lone pair of electrons on each oxygen atom of the o-semiquinone is used in the bonding to the metal.

The molecular structures of Cu^{2+} and Fe^{3+}-catechol model complexes have been proposed using FTIR spectra study and elemental analysis data. We have found that the metal- polymeric quinone and semiquinone complexes are formed at condition I while the metal - polymeric semiquinone complexes formed at condition II and the metal-catecholate or semiquinone complexes formed at condition III. Although each model structure is not the unique structure of these complicated catechol-Cu^{2+} and Fe^{3+} complexes, the structures proposed here fit our FTIR data, ESR spectra, and element analysis results.

The comparison of the behaviors of the model catechol molecule and the AHA in terms of the coordination site selectivity, coordination mechanism, and coordination ability all indicates that the polymerization of catechol is reminiscent to what is seen in the AHA, making catechol an acceptable model compound for the study of AHA.

Reference

1. Suffet, I. H.; MacCarthy, P. *Aquatic Humic Substances. Influence on Fate and Treatment of Pollutants* American Chemical Society, Washington, DC **1989**.

2. Caron, G.; Suffet, I. H. *Abstracts of Papers*. 193 rd National Meeting of the American Chemical Society, Denver, Co; American Chemical Society: Washington, DC, **1987**;ENVR 5.

3. Hart, B. T. *Environ. Technol. Lett.* **1981**, 2, 95-110.

4. Szilagyi, M. *Fuel.* **1974,** 53, 26.

5. Lobartini, J. C.; Tan, D. H. *Soil Sci. Soc. Am. J.* **1988,** 52, 125-130.

6. Chiou, C. T.; Porter, P. E.; Schmedding, D. W. *Environ. Sci. Technol.* **1983**, 17, 227-231.

7. Garbarini, D. R.; Lion, l. W. *Environ. Sci. technol.* **1986**, 20, 1263-1269.

8. Stevenson, F. J. *Humus Chemistry* John Wiley & sons: New York, **1982**, 45.
   Bulet. **1982**, 1, 1457.

9. Pierpont, C. G.; Lange, C. W. *The Chemistry of Transtion Metal Complexes Containing Catechol and Semiquinone ligands*. Department of Chemistry and Biochemistry. University of Colorado. Boulder, Colorado.**1994**

10. Milorad, M. R.; Timothy, R. D. *J. Am. Chem. Soc.* **1978**, 100:17, August 16, 5472.

11. Brubaker, C. H. Jr.; Wicholas,M. *J. Inorg. Nucl. Chem.* **1965,** 27, 59.

12. Cornel, P. K.; Summers, R. S.; Roberts, P. V. *J. Colloid Interface Sci.***1986**, 110, 149-164.

13. Tsutsuki, K.; Kuwatsuka, S. *Soil Sci. Plant Nutr.* **1984**, 30, 151-162.

14. Davis, J. A. *Geochim. Cosmochim. Acta.* **1982**, 46, 2381-2393.

15. Tipping, E.; Cooke, D. *Geochim. Cosmochim. Acta.* **1982**, 46, 75-80.

16. Cordes, M. M.; Walter, J. L. *Spectrochimica Acta.* **1968**, 24A, 1421-1435.

17. Colthup, N. B.; Daly, L. H.; Wiberley, S. E. *Introduction to Infrared and Raman Spectroscopy*. Academic press, Inc. **1990.**

18. Bellamy, L. J. *The Infrared Spectra of Complex Molecules* John Wiley & Sons, Inc. New York. **1954.**

19. Reinprecht, j. T. ; Vogel, G. C. *Inorg. Nucl. Chem. Letters.* **1976**, 12, 399-404.

20. Bohel, S. D.; Carron, K. T.; Christensen, N. A. ; Goodson, P. A.; Powell, A. K.

Organometallics **1994**, 13, 1355-1373.

21. Lynch, M. W.; Valentine, M.; Hendrickson, D. N. *J. Am. Chem. Soc.* **1982,** 104, 6982-6989.

22. Jones, R. N.; Humphries, P.; Dobriner, K. *J. Amer. Chem. Soc.* **1950**, 72, 956.

23. Lever, A. B. P.; Auburn, P. R.; Dodsworth, E. S.; Masa-aki-Haga; Wei Liu; Melink, M.; Nevin, W. A. *J. Am. Chem. Soc.* **1988**, 110, 8076-8084.

24. Blaakmeer, J.; Bohmer, M. R. Cohen, Stuart, M.A.; fleer, G. J. *Macromolecules* **1990,**23, 2301-2309.

25. Foissy, A.; Elattar, A.; Lamarche, J. M. *J. Colloid Interface Sci.* **1983**, 96, 275-287.

26. Van der Schee, H. A.; Lyklema, J. *J. Phys. Chem.* **1984**, 88, 6661-6667.

27. Cafe, M. C.; Robb, I. D. *J. Colloid Interface Sci.* **1982**, 86, 411-421.

28. Bohmer, M. R.; Evers, O. A.; Scheutjens, J. M. H. M. *Macromolecules* **1990**, 23, 2288-2301.

29. Huheey, J.E. *Inorganic Chemistry Principles of Structure and Reactivity* harper & Row, Publishers New York. **1978**.

30. Hadjiioannou, T. P.; Christian, G. D.; Efstathiou, C. E.; Nikolelis, D. P. *Problem Solving in Analytical Chemistry* Pergamon Press. **1988.**

31. Bailey, S. I.; Ritchie, I.M. *J. Chem. Soc. Perkin Trans. II* **1983**, 645-652.

32. Ilan, Y. A.; Gidon Czapski; Meisel, D. *Biochimica et Biophysica Acta,* **1976,** 430, 209-224.

33. Timothy, R.; Demmin, M. D. Rogic, M. M. *J. Am. Chem. Soc.* **1981**, 103, 5795-5804.

34. Hashimoto, H.; Noma, T.; Kawaki, T. *Tetrahedron lett.* **1968**, 3411.

35. Hay, P. J.; Thibeault, J. C.; Hoffmann, R. *J. Am. Chem. Soc.* **1975,** 97, 4884.

36. Adams, R. W.; Bishop, E.; Martin, R. L.; Winter, G. Aust. *J. Chem.* **1966**, 19, 207.

37. Odian, G. C. *Priciples of Polymerization* MeGraw-Hill Book company New York. **1970.**

38. Michael H. B. Hayes; Patrick Maccarthy; Malcolm, R. L.; Roger S. Swift *Humic Substances II In Search of Structure* John Wiley & Sons New York. **1989.**

39. Buchanan, R. M.; Kessel, S. L.; Downs, H. H.; Pierpont, C. G.; and Hendrickson, D. N. *Journal of the American Chemical Society* 100:25 Dec, 6, **1978**.

40. Pople, J. A.; Beveridge, D. L.; and Dobosh, P. A. *J. Am. Chem.Soc.* 90, 4201, **1968;** Edwards,T.G.; and Ginter, R. *Mol. Phys.* 15, 367, **1968**; Kikuchi, O. and Someno,K. *Bull. Chem. Soc. Jpn.* 40, 2972, **1967**; pedersen, J. A. and Larsen, J. S. *Chem. Phys.Lett.* 35, 41,**1975.**

CHAPTER IV

Future Work

4.1 ESR Study on AHA, AHA-Metal Complexation

We have demonstrated the use of ESR spectroscopy in association with FTIR to identify the structure of metal-catechol model complexes. Specifically, the ESR spectrum can determine the nature of Cu^{2+} ion, semiquinone radicals in the polymer and complexation of catechol with metal ions by characteristic g-values and hyperfine structure.

Further ESR studies on AHAs and metal-AHA complexes are based on the assumption of a quinone-hydroquinone moiety within the AHA macromolecule. [1] The results of numerous investigations during the past 20 years support the hypothesis of free radical species. In addition, recent investigations of Senesi[2] and others have revealed the nature of the interactions of these free radicals with organic and inorganic species in environment. The application of ESR spectroscopy has been invaluable in these studies.

ESR spectral parameters of AHA, such as spin density, g-factors, and hyperfine structure, can be used to characterize and follow the reactivity of AHA. The pH, temperature, reduction-oxidation, hydrolysis, and irradiation affect the ESR properties of AHA, which increase the complexity of the study.

These results can be explained in terms of a series of competing reactions (Figure 4.1):
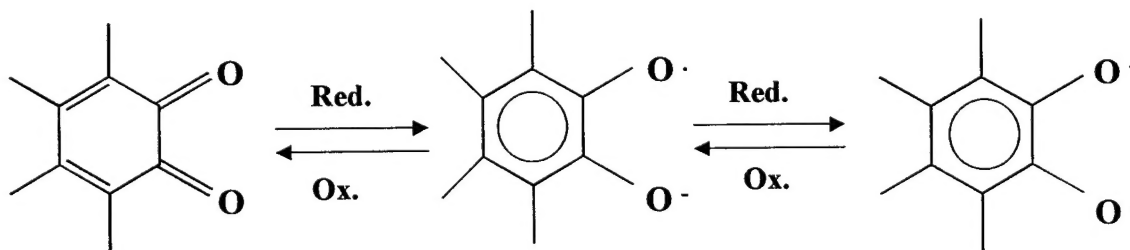

Figure 4.1 Scheme of quinone-hydroquinone reversible reactions

In this future work, ESR spectra of AHA subjected to the oxidation-reduction of AHA with metal ion

61

Cu^{2+} and Fe^{3+} at acidic condition will be acquired. Previous work of this research has described the oxidation and complexation of AHA in the presence of metal ions as determined by FTIR spectroscopy. The application of ESR spectroscopy associated with FTIR spectroscopy should furnish useful information about (1) the nature of the polymerization and humification process of AHA, and (2) their role as activator of adsorption of natural inorganic and organic species in environment.

4.2 Partition Study of AHA-Benzene Derivatives by HPLC

A large fraction of waste chemicals contained in groundwater consist of hydrophobic organic compounds from the petroleum industry. Many of the chemical wastes are benzene derivatives. The role that HA may play in the transport, reactivity, and fate of these hydrophobic organic compounds has been summarized by Caron and Suffet. [3] It has been shown that the degree of association is affected by the nature of the compounds and HA, their concentration, pH, and the presence of other organic and ionic solute. The octanol-water partition coefficient (K_{ow}) is widely used for predicting the degree of association. Attempts to correlate the degree of association with measurable characteristics of HA have not been very successful and Caron and Suffet point out the shortcomings of the widespread practice of using natural HA and commercial HA for studies of association. Our development of reliable methods for predicting the association between hydrophobic organic waste compounds and the AHA will be very useful in predicting the fates of the wastes.

The work we performed to date on metal ion interactions with humic materials will be extended to association of organic materials with AHA. We will attempt to develop HPLC techniques that allow us to determine the partition properties of organics into AHA. It should be possible to use reverse-phase methods to develop distinguishing retention times between partition aromatics and free aromatics. A diode array detector will be used to spectroscopically distinguish between partition aromatics and free aromatics. Several possible approaches to the analysis will be examined. For example, one may be able to examine both the thermodynamic and kinetic properties of sorption of organic materials by AHA. Gradient of aromatic concentration in an aqueous solution in a binary flow system with a constant AHA concentration should lead to a thermodynamic determination of the isotherm. Variation of pH, temperature, and ionic strength of the flow system will allow us to ascertain the roles that these variable play in the sorption of aromatics. This of

course depends on our ability to spectrally distinguish between free and sorbed aromatics. Kinetic studies can be performed by injecting aromatic/AHA complexes and using the retention of the column to separate the AHA from the aromatics. Variation of flow rate (retention time) should allow one to determine the rate of desorption of the aromatic from the AHA.

The characteristics of the adsorption isotherms which are plot as [pollutants]$_{solution}$ vs [pollutants]$_{AHA}$ (Figure 4.2) .
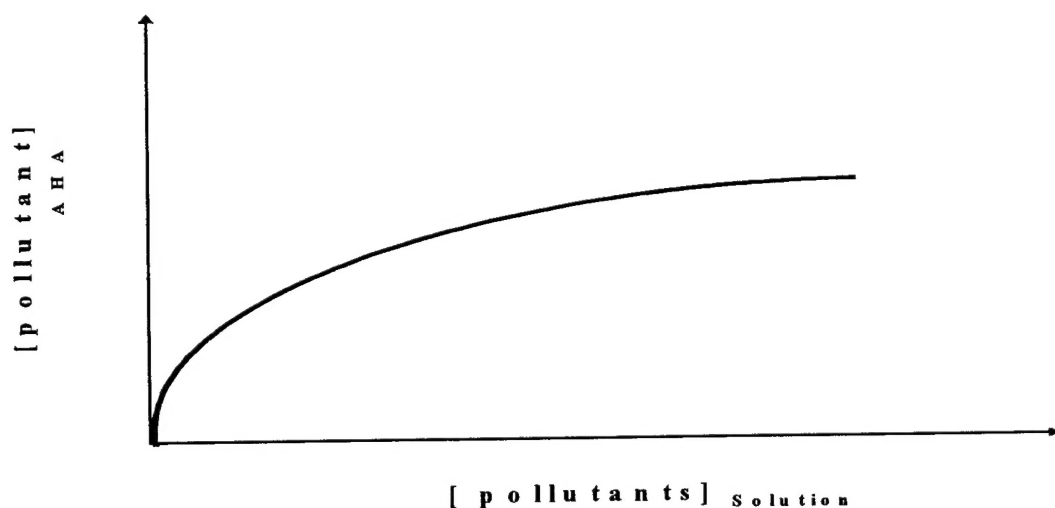
Figure   **4.2**

Adsorption isotherms of AHA with benzene pollutants

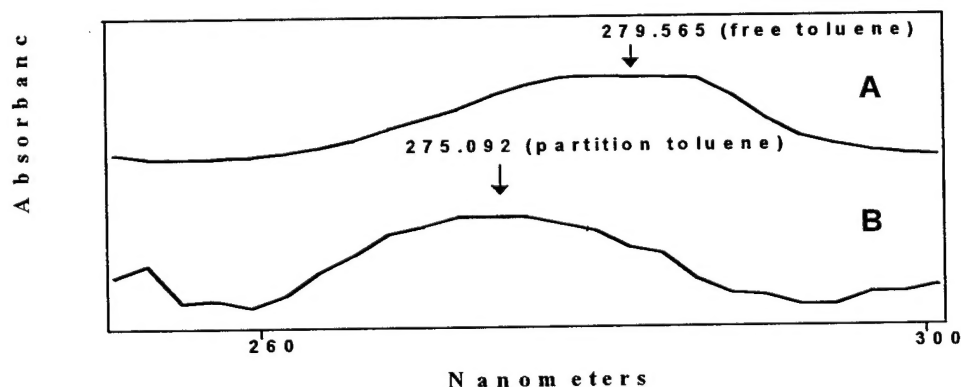The UV spectra of partition toluene on AHA and free toluene in water are showed in Figure 4.3.

Figure 4.3 UV spectra of (A) toluene and (B) AHA-toluene

63

We will also attempt to correlate the partition ability of pollutants with the structure characteristics, solubility, and polarity of AHA. Previous work in this research has described that the structure form of AHA is affected by the solution pH, temperature, and the oxidization-reduction effect. Therefore, it is obvious that the partition ability of organic pollutants on AHA should be affected by those factors. The application of HPLC spectroscopy in these investigation should give us better understanding about the partition mechanisms and the fates of pollutants.

Reference

1. Steelink, C.; Tollin, G. *Biochem. Biophys. Acta.* **1962,** 59, 25-34.

2. Senesi, N.; Schnitzer, M. *Environmental Biogeochemistry and Geomicrobiology* Ann Arbor Science, Ann Arbor, MI, p 467-481.

3. Caron, G.; Suffet, I. H. *Abstracts of Papers, 193rd National Meeting of the American Chemical Society,* Denver, CO; American Chemical Society: Washington, DC, **1987,** Vol.27, No.1, 286-288.